

# Thesis

Ekaterina Avdeeva

University of Nebraska-Lincoln, USA

December 19, 2016

## Abstract

This paper reviews

## Contents

8	<b>1</b>	<b>Introduction</b>	<b>2</b>
9	1.1	Fundamental Particles and Interactions . . . . .	3
10	1.2	Electroweak Interactions . . . . .	5
11	1.3	Strong Interactions . . . . .	8
12	1.4	Physics of Proton-Proton Collisions . . . . .	9
13	1.5	Open Questions of the Standard Model . . . . .	11
14	<b>2</b>	<b><math>W\gamma</math> Production Theory and Former Experimental Results</b>	<b>12</b>
15	2.1	Electroweak Theory of the Standard Model . . . . .	13
16	2.2	Cross Section and Luminosity . . . . .	18
17	2.3	Standard Model $W\gamma$ Production . . . . .	20
18	2.4	Anomalous $W\gamma$ Production . . . . .	23
19	2.5	Measurements in the Past . . . . .	25
20	<b>3</b>	<b>Experimental Setup</b>	<b>27</b>
21	3.1	Large Hadron Collider . . . . .	28
22	3.2	Compact Muon Solenoid . . . . .	31
23	3.2.1	Introduction . . . . .	31
24	3.2.2	Magnet . . . . .	32
25	3.2.3	Tracking System . . . . .	32
26	3.2.4	Electromagnetic Calorimeter . . . . .	33
27	3.2.5	Hadron Calorimeter . . . . .	34
28	3.2.6	Muon System . . . . .	34
29	3.2.7	Triggering and Data Aquisition . . . . .	35
30	3.2.8	Event Reconstruction . . . . .	35
31	<b>4</b>	<b>CMS Tracker Alignment</b>	<b>38</b>
32	4.1	Algorithm . . . . .	39
33	4.2	Selected Results . . . . .	44
34	<b>5</b>	<b><math>W\gamma</math> Cross Section Measurement</b>	<b>45</b>

## 35    1 Introduction

36    Elementary particle physics describes fundamental particles and their interactions. Fundamental  
37    particles are the smallest constituents of our Universe. When examined at smaller scales, the  
38    substances around us consist of molecules, molecules consist of atoms. In an atom there is a  
39    nucleus made of neutrons and protons and some number of electrons occupying orbits around  
40    the nucleus. Protons and neutrons have a structure while an electron is not known to have any  
41    internal structure, therefore, an electron is an example of a particle which is considered to be  
42    fundamental.

43

44    Interactions of elementary particles are described by quantum field theories which incorporate  
45    principles of the quantum mechanics and the special theory of relativity. The set of such theories,  
46    including quantum elecrtrodynamics (QED), quantum chromodynamics (QCD) and the theory  
47    of weak interactions is called the Standard Model (SM). Current observations have proved the  
48    SM to be an accurate description of elementary particle interactions.

49

50    However, there are several experimental observations that are not described by the SM such  
51    as effects of gravity, dark matter, dark energy, matter/antimatter asymmetry and others. There-  
52    fore, the SM is not the complete theory of particle interactions. There are several SM extensions  
53    offered by theorists as well as radically new theories waiting for experimental confirmation or  
54    exclusion.

55

56    Some SM extensions and new theories predict the existence of heavy particles with masses  
57    lying beyond experimentally reachable energies. The search of these particles is a priority in  
58    particle physics. One source of highly energetic elementary particles is cosmic rays. The most  
59    energetic particles ever observed came from this source. However, cosmic rays are totally uncon-  
60    trollable and such highly energetic particles are rare. If we want to produce a large number of  
61    particles in a given energy range, we need to use a particle accelerator. A large amount of data  
62    allows experimentalists to perform a statistical analysis and increase the probability of finding a  
63    new particle if it exists.

64

65    Symmetric colliding beams is the most effective way to produce as heavy particles as possible  
66    given the energies of the colliding particles. Compared to experiments colliding a single beam at  
67    a fixed target, in the case of a symmetric collision the total momentum of two colliding particles  
68    is zero and, therefore, much larger fraction of energy can transfer to a mass of a new particle.  
69    The Large Hadron Collider (LHC) is one such collider with the highest energy in the world. It  
70    can produce the most massive particles to probe physics beyond the SM (BSM).

71

72    The Compact Muon Solenoid (CMS) is one of two general-purpose detectors at the LHC. It  
73    is placed at one of four collision points. CMS has a broad physics program including searches for  
74    the BSM physics as well as the precision measurements of the parameters of the SM itself. The  
75    measurement of this dissertation is a SM measurement with CMS data collected in 2012 in  $pp$   
76    collisions of LHC with beam energies of 4 TeV. The result can be compared to the SM prediction.  
77    Certain BSM theories predict a deviation of the result of this measurement from its SM value,  
78    therefore, with this measurement, in addition to testing the SM, we also search for a new physics.

79

80    The rest of this chapter gives general introductory information about the SM while Ch. 2  
81    concentrates on the theory of the SM and BSM  $W\gamma$  production and also discusses previous  
82    measurements of this process. Chapter 3 describes LHC and CMS in more details. Chapter 4  
83    explains one specific detail of the CMS operation that is the spacial alignment of the tracking  
84    detector of charged particles. Finally, Ch. 5 describes the details of the measurement of this  
85    dissertation and reports the results.

86

## 87 1.1 Fundamental Particles and Interactions

88 The SM describes interactions of elementary particles. There are four fundamental interactions:  
89 electromagnetic, strong, weak and gravitational. The gravity is not included into the SM but its  
90 effect on particles is negligible compared to the other forces which makes it possible to develop a  
91 theory of the particle physics and conduct experiments even without having the gravity included  
92 into the model.

93  
94 All fundamental elementary particles in the SM can be split into three categories by their  
95 spins. There are fermions which possess spin  $s=1/2$ , there are gauge bosons which are vector  
96 particles ( $s=1$ ) and there is the Higgs boson which is a scalar particle ( $s=0$ ).

97  
98 The fermions are arranged into three generations, each generation consists of a quark with  
99 charge  $Q=+2/3$  (up, charm, and top quarks), a quark with  $Q=-1/3$  (down, strange, and bottom  
100 quarks), a charged lepton with  $Q=-1$  (electron, muon, and tau-lepton) and a neutrino (electron,  
101 muon, and tau neutrinos) which is electrically neutral. Each quark can carry any of three colors:  
102 red, blue, or green. Additionally, each fermion has its antiparticle. Therefore, the total number  
103 of fundamental fermions is  $(6(\text{leptons}) + 6(\text{quarks}) \cdot 3(\text{colors})) \cdot 2(\text{to include antiparticles}) = 48$ .

104  
105 Corresponding particles in different generations have the same charges, spins and interaction  
106 properties but masses of particles increase with a generation. These mass differences lead  
107 to different decay properties because a particle A can decay to particles B and C only if their  
108 masses relate as  $m_A > m_B + m_C$ . Thus, an electron is a stable particle, a muon decays as  
109  $\mu^- \rightarrow e^- + \bar{\nu}_e + \nu_\mu$ , a tau-lepton, as the heaviest charged lepton, has the largest number of decay  
110 channels amongst the charged leptons:  $\tau^- \rightarrow \mu^- + \bar{\nu}_\mu + \nu_\tau$ ,  $\tau^- \rightarrow e^- + \bar{\nu}_e + \nu_\tau$ ,  $\tau^- \rightarrow \nu_\tau + \text{quarks}$ .

111  
112 In addition to fermions, the SM includes gauge bosons which are interaction mediators. They  
113 are called mediators because fermions interact with each other by exchanging them. For example,  
114 two charged fermions can interact with each other by exchanging a photon. Such interaction is  
115 called electromagnetic interaction and a photon is a mediator for the electromagnetic interaction.  
116 Similarly, a gluon is a mediator for strong interactions, and  $W^\pm$  and  $Z^0$  bosons are mediators  
117 for weak interactions.  $W^\pm$  and  $Z^0$  bosons are massive while a photon and a gluon are massless  
118 particles.

119  
120 The last SM particle is the Higgs boson. The Higgs boson is a scalar neutral particle which  
121 is playing a critical role in the electroweak symmetry breaking. The Higgs mechanism explains  
122 how  $W$  and  $Z$  bosons become massive particles.

123  
124 All the particles are summarized in Fig. 1. These and only these fundamental particles and  
125 their antiparticles have been discovered by now. However, there are many composite particles  
126 which are called hadrons. Hadrons can consist of three quarks (baryons), quark and antiquark  
127 (meson), or three antiquarks (antibaryons). Hadrons always possess an integer charge.

128  
129 Most of the particles are short-lived and decay within microseconds. The only stable particles  
130 are protons and antiprotons, electrons and positrons, neutrinos and antineutrinos, photons,  
131 and, in some sense, gluons. However, if a particle cannot decay, it does not mean that it would  
132 live forever. There are many different kinds of reactions in which particles can disappear. An-  
133 tiprotons and positrons would immediately annihilate with protons and electrons, photons can  
134 be absorbed by charged particles, electrons and protons can scatter to produce neutrons and  
135 neutrinos and many other reactions are possible.

136  
137 In this dissertation, the study of  $pp \rightarrow W\gamma + X \rightarrow l\nu\gamma$  process where  $l = e, \mu$  is presented. The  
138  $W\gamma$  production with leptonic  $W$  decays proceeds through one of the following three processes:  
139 the initial state radiation where a photon is emitted from one of the incoming partons, the final  
140 state radiation where a photon is radiated off the charged lepton from the  $W$  boson decay, and,  
141 finally, the triple gauge coupling (TGC) where a photon is emitted from the  $W$  boson. Many

142 BSM theories predict an enhancement of the TGC production over the SM value and, therefore,  
 143 the experimental search for such an enhancement is a good test for such theories.

144  
 145 Therefore, the focus of this study is an interaction between a photon and a  $W$  boson however  
 146 many other SM particles are relevant too. Thus, a charged lepton and a neutrino appear as the  
 147 final state particles, a quark and an antiquark appear as initial state particles and all fundamental  
 148 particles except the Higgs boson participate in various background processes. Subsequent  
 149 chapters describe these particle interactions in more details.

150

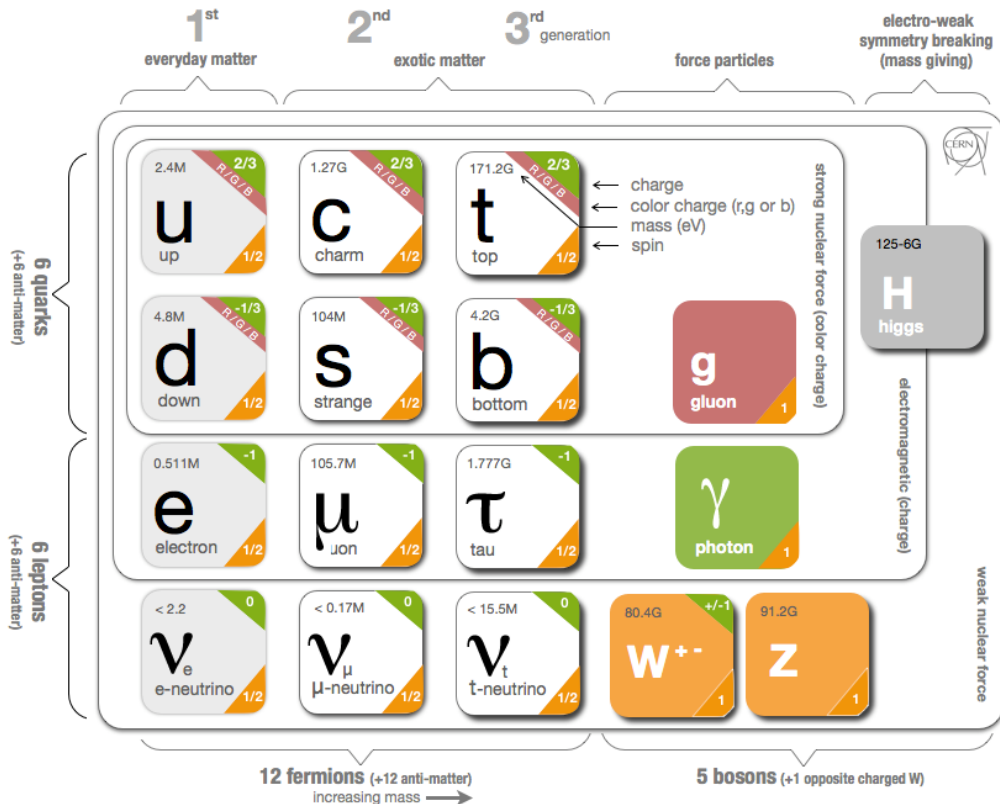


Figure 1: Standard Model Particles and Interactions. Source of the figure: [2].

151 **1.2 Electroweak Interactions**

152 All electrically charged particles participate in electromagnetic interactions. The theory of elec-  
 153 tromagnetic interactions is called quantum electrodynamics (QED). All electromagnetic inter-  
 154 actions are mediated by a photon, a spin-one electrically neutral massless particle, and can be  
 155 reduced to one elementary process (Fig. 2, left). This process represents a charged fermion  
 156 radiating or absorbing a photon. Such elementary process itself is forbidden by the energy con-  
 157 servation law but this element is a base of an actual process. For example, the Bhabha scattering,  
 158  $e^+e^- \rightarrow e^+e^-$ , occurs through  $e^+e^-$  annihilation with further production of a new  $e^+e^-$  pair  
 159 (Fig. 2, middle) or through exchange of a photon between the positron and the electron (Fig. 2,  
 160 right). Both cases involve nothing except the electromagnetic elementary process (Fig. 2, left).  
 161 Such graphical representations of the particle physics processes are called Feynman diagrams.

162

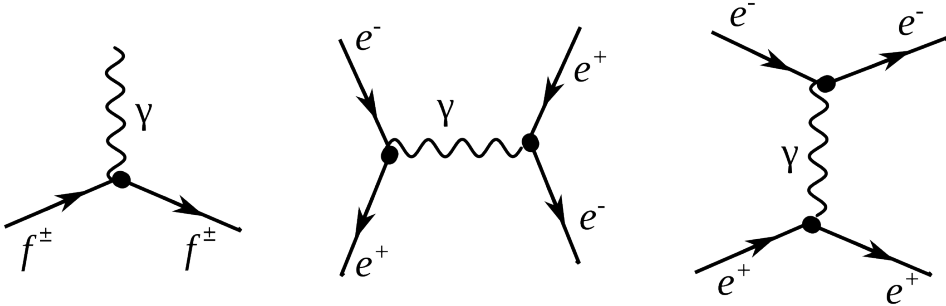


Figure 2: Electromagnetic interactions. Left: a photon radiation off a charged fermion, middle and right: Bhabha scattering.

163 As for the weak interactions, there are two kinds of them: neutral (mediated by a  $Z$  boson)  
 164 and charged (mediated by a  $W^\pm$  boson). Elementary processes with  $W$  and  $Z$  bosons are shown  
 165 in Fig. 3. Because the electric charge must be conserved at any vertex, a particle radiating or  
 166 absorbing a  $W$  boson converts to a different particle. Thus, a charged lepton converts to a neu-  
 167 trino (or vice versa) as shown in Fig. 3, top middle. Each lepton carries a lepton flavor number  
 168 (Tab. 1). Lepton flavor is conserved in any interaction, thus an electron radiating a  $W$  boson  
 169 always converts to an electron neutrino, a muon converts to a muon neutrino etc.

170

Table 1: Lepton Flavor Number

particles	$L_e$	$L_\mu$	$L_\tau$
$e^-, \nu_e$	+1	0	0
$e^+, \bar{\nu}_e$	-1	0	0
$\mu^-, \nu_\mu$	0	+1	0
$\mu^+, \bar{\nu}_\mu$	0	-1	0
$\tau^-, \nu_\tau$	0	0	+1
$\tau^+, \bar{\nu}_\tau$	0	0	-1

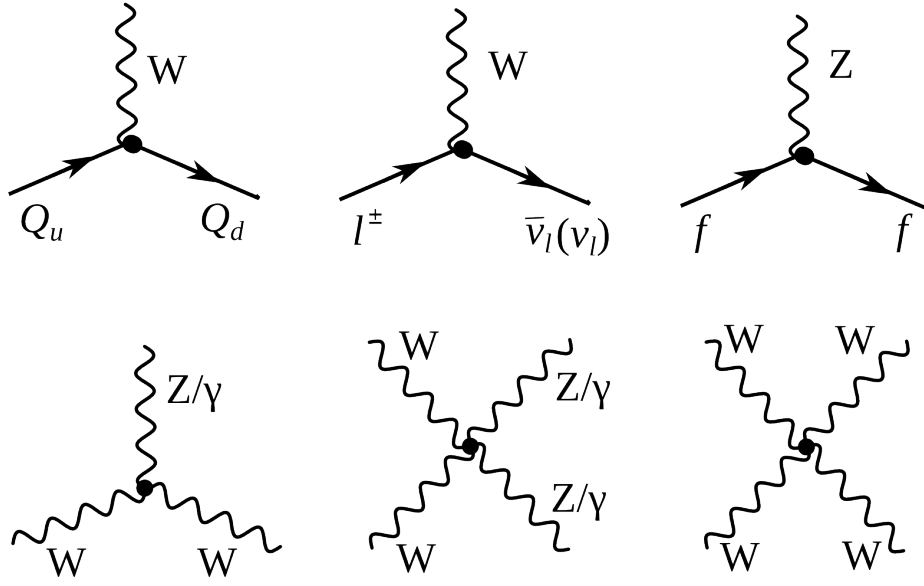


Figure 3: Weak elementary processes and gauge couplings. Top left: a quark with charge  $Q=+2/3$  enters, emits a  $W$  boson, and a quark with charge  $Q=-1/3$  escapes. Top middle: a charged lepton enters, emits a  $W$  boson, and a neutrino or antineutrino escapes conserving a lepton flavor number. Top right: a fermion enters, emits a  $Z$  boson and escapes. Bottom left: TGC couplings  $WW\gamma$  and  $WWZ$ . Bottom middle: QGC couplings  $WW\gamma\gamma$ ,  $WWZ\gamma$  and  $WWZZ$ . Bottom right: QGC coupling  $WWWW$ .

From top left diagram in Fig. 3 we see that if a quark with  $Q=+2/3$  enters, then a quark with  $Q=-1/3$  escapes and, therefore, the flavor of the quark is changed. The charged weak interaction is the only interaction which changes a quark flavor. The probability of each of three quarks with  $Q=-1/3$  to be born is determined by the Cabibbo-Kobayashi-Maskawa matrix which relates mass eigenstates  $d$ ,  $c$  and  $b$  to weak eigenstates  $d'$ ,  $c'$  and  $b'$  (Eq. 1). Absolute values of the matrix elements are all known (Eq. 2) and are the highest for the quark of the same generation as an initial state quark. In the particular case shown in the top left diagram in Fig. 3,  $u$  is the initial state quark and  $d$  has the highest probability to be produced after an interaction with a  $W$  boson but  $s$  and  $b$  can also be produced if there is enough energy.

180

$$\begin{pmatrix} d' \\ s' \\ b' \end{pmatrix} = \begin{pmatrix} V_{ud} & V_{us} & V_{ub} \\ V_{cd} & V_{cs} & V_{cb} \\ V_{td} & V_{ts} & V_{tb} \end{pmatrix} \begin{pmatrix} d \\ s \\ b \end{pmatrix} \quad (1)$$

$$\begin{pmatrix} |V_{ud}| & |V_{us}| & |V_{ub}| \\ |V_{cd}| & |V_{cs}| & |V_{cb}| \\ |V_{td}| & |V_{ts}| & |V_{tb}| \end{pmatrix} = \begin{pmatrix} 0.97 & 0.23 & 0.00 \\ 0.23 & 0.97 & 0.04 \\ 0.01 & 0.04 & 1.00 \end{pmatrix} \quad (2)$$

An elementary process of a neutral weak interaction is an emission a  $Z$  boson off a fermion line (right top diagram in Fig. 3). Diagrams with a  $Z$  boson are very similar to ones with a photon except a photon can only be radiated off a charged particle but a  $Z$  boson can also be radiated off a neutrino or antineutrino.

185

186 The bottom diagrams in Fig. 3 are gauge bosons coupling diagrams including self-coupling  
 187 of a  $W$  boson, its interaction with a  $Z$  boson and its electromagnetic radiation of a photon.  
 188 Charge-conserving TGC and quartic gauge couplings (QGC) containing two or four  $W$  bosons  
 189 are all possible in the SM:  $WWZ$ ,  $WW\gamma$ ,  $WWZZ$ ,  $WWZ\gamma$ ,  $WW\gamma\gamma$ , and  $WWWW$ .  
 190

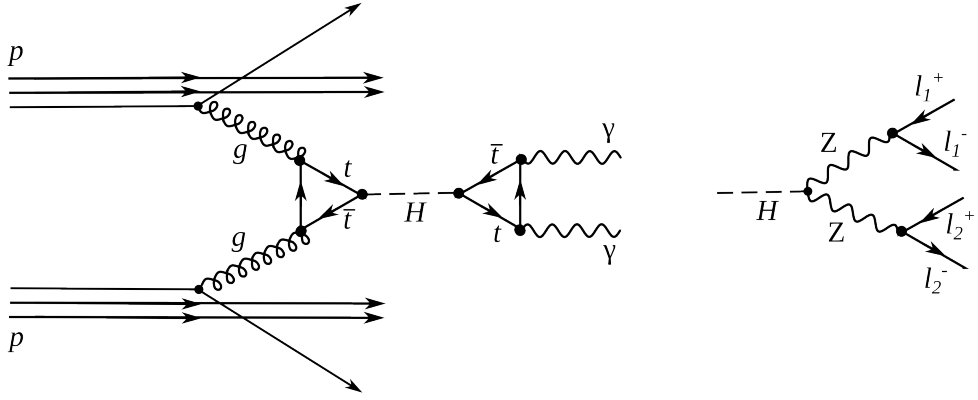


Figure 4: The Higgs boson production and decay. Left:  $H \rightarrow \gamma\gamma$ , right:  $H \rightarrow ZZ \rightarrow 4l$ .

191 Electromagnetic and weak interactions are unified by the electroweak Glashow-Weinberg-  
 192 Salam (GWS) theory which is based on  $SU(2) \times U(1)$  symmetry.  $SU(2)$  is the symmetry of  
 193 weak isospin which generates three bosons:  $W^1$ ,  $W^2$  and  $W^3$ .  $U(1)$  is the symmetry of the weak  
 194 hypercharge and generate one neutral boson  $B$ .  $W^1$  and  $W^2$  are mixed to create  $W^+$  and  $W^-$   
 195 mediators while  $W^3$  and  $B$  are mixed to create a  $Z$  boson and a photon. Therefore, the GWS  
 196 theory considers electromagnetic and weak forces as different manifestations of the electroweak  
 197 force. The electroweak theory is discussed in greater details in Ch. 2.

198 However, weak interactions are mediated by heavy bosons ( $M_W = 80$  GeV,  $M_Z = 91$  GeV)  
 199 while electromagnetic interactions are mediated by a massless photon, thus, the electroweak  
 200 symmetry is broken. To explain this phenomenon, the Higgs mechanism was introduced. The  
 201 mechanism predicted an existence of an additional boson: the Higgs boson. The Higgs boson  
 202 was a missing piece of the SM for many years and was finally discovered in 2012 at LHC by  
 203 ATLAS and CMS collaborations through the processes shown in Fig. 4 [3], [4].  
 204

205 The measurement in this dissertation is an electroweak measurement because the process  
 206 involves a  $W$  boson. It includes an interaction of a  $W$  boson with leptons and quarks as well as  
 207 the TGC  $WW\gamma$ . Thus, the measurement is a good test of the SM electroweak theory.  
 208

209

---

210 1.3 Strong Interactions

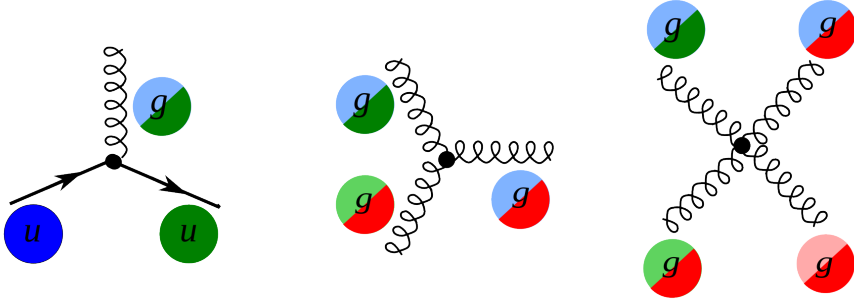


Figure 5: Elementary processes of strong interactions

211 The third fundamental force after the electromagnetic and weak ones is the strong force. The  
212 strong force is responsible for gluing protons and neutrons together in the nuclei as well as for  
213 forming protons and neutrons themselves. The strong interactions occur by exchanging gluons  
214 which are spin-one massless electrically neutral particles.

215

216 The elementary strong processes are shown in Fig. 5. There are three elementary processes:  
217  $qqg$ ,  $ggg$  and  $gggg$ , all are involving particles with color charges. Thus, gluons couple to quarks  
218 and self-couple. Color charges must be conserved at each elementary process of the strong inter-  
219 action. Each quark possesses one of three colors at a time, and there are eight types of gluons  
220 to cover all possible color exchanges.

221

222 The coupling constant of the strong interaction depends on a distance between interacting  
223 particles: it becomes larger as the distance becomes larger and smaller as the distance becomes  
224 smaller. As the distance approaches zero, the coupling constant approaches zero too, and, thus,  
225 in the asymptotic limit two quarks located at the same place do not interact. This property is  
226 called asymptotic freedom.

227

228 On the other hand, when the distance between quarks becomes larger, the coupling constant  
229 also becomes larger. This property confines quarks to always stay in the color neutral combi-  
230 nations (hadrons), it forbids the existence of free quarks. A combination becomes color neutral  
231 when there is the same amount of color and anticolor or if there is the same amount of each of  
232 the three colors. Thus, mesons are comprised of a quark and an antiquark with the opposite  
233 color charges, and baryons are comprised of three quarks: red, green and blue one. Examples of  
234 baryons include such well-known particles as a proton and a neutron.

235

236 The asymptotic freedom and the confinement are properties that are specific for strong inter-  
237 actions. The theory of strong interactions is called the quantum chromodynamics (QCD)  
238 which is a quantum field theory invariant under  $SU(3)$  color transformations. When the cou-  
239 pling constant is much less than one  $\alpha_s \ll 1$ , the perturbative approach can be used to compute  
240 observables.

241

242 The  $W\gamma$  process being measured in this dissertation is not intended to test QCD, but a good  
243 understanding of QCD is essential for performing this measurement because the QCD correc-  
244 tions to the Feynman diagrams of the process are large and have to be taken into account when  
245 producing simulation. In addition, QCD describes the dynamics of quarks and gluons within  
246 colliding protons and predicts probabilities of one or another quark-antiquark pair to interact.  
247 Physics of proton-proton collisions is discussed in the Ch. 1.4.

## 249 1.4 Physics of Proton-Proton Collisions

250 Consider a  $pp$  collision at LHC. The proton energies are so high that each proton behaves as a  
 251 complex structure. A proton is a baryon, it consists of three quarks:  $uud$ . These three quarks  
 252 are called valence quarks. They interact with each other by exchanging gluons which produce  
 253 virtual  $q\bar{q}$  pairs (Fig. 6). Such quarks are called sea quarks.

254 Any parton from one proton can interact with any parton from another proton. Probabilities  
 255  $f_i(x, Q^2)$  of any particular constituent  $i$  to interact are described partially by QCD and parti-  
 256 cally by experimental measurements and depend on the momentum transfer  $Q$  and the momen-  
 257 tum fraction of a specific parton  $x$ . These probabilities are called parton distribution func-  
 258 tions (PDFs).

260

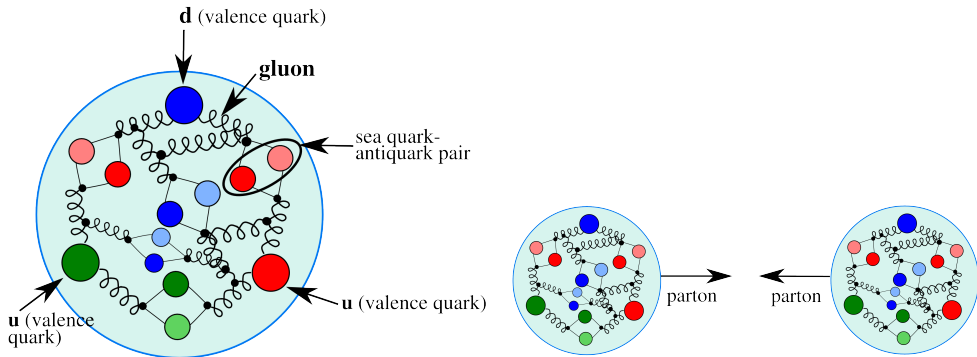


Figure 6: The proton structure (left) and the proton-proton collision (right).

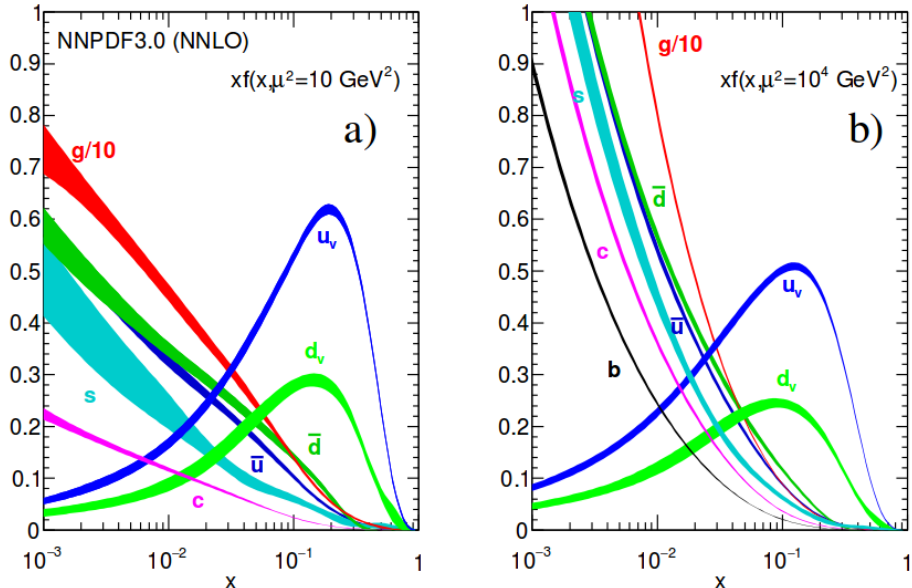


Figure 7: Parton distribution functions [5].

261 For large  $Q^2$  and  $x$  gluon-gluon interactions have the largest probabilities to occur (Fig. 7).

262 However, gluons do not couple directly to a  $W$  boson, thus, in the  $W\gamma$  measurement we are  
263 mostly interested in quark-antiquark pairs which would have a total charge corresponding to the  
264 charge of a  $W$  boson ( $\pm 1$ ). Since we have  $u$  and  $d$  as valence quarks and we know that the  
265 probability to couple to the same generation quark in charged weak interactions is the highest,  
266 most of the  $W$  bosons are created by  $u\bar{d}$  and  $d\bar{u}$  pairs however other  $q\bar{q}'$  combinations with the  
267 total charges of  $\pm 1$  are also possible. As we look for events containing  $W\gamma$  we also have other  
268 events mimicking our process. Such background events can be produced by any pair of partons.

269

## 270 1.5 Open Questions of the Standard Model

271 While the SM is an accurate description of all particle physics experimental results, there are  
272 certain phenomena which are not included into the SM. In this subsection we discuss some of  
273 them.

274 The gravitational interactions do not fit into the SM. It is the open question whether the  
275 quantum theory of gravity is possible and whether there is a mediator of the gravitational in-  
276 teractions. Also, it is not known why the gravitational force is so much weaker than the other  
277 forces. One possible explanation comes from a theory which predicts extra spatial dimensions  
278 beyond the three we experience (e.g. the string theory). In this case, it is possible that the  
279 gravitational force is shared with other dimensions and only a fraction is available in our three  
280 dimensions.  
281

282 Another mystery of the universe is its composition: it is known from the studies of the grav-  
283 itational effects that our universe consists of dark energy by 68%, of dark matter by 27% and of  
284 baryon matter only by 5% [6]. The dark energy resists the gravitational attraction and acceler-  
285 ates the expansion of the universe, and is not detectable by any effects except gravitational. The  
286 understanding of dark energy is a question of general relativity rather than particle physics. The  
287 dark matter, however, likely consists of particles and therefore is a subject of particle physics.  
288 It does not radiate and that is why it cannot be detected by telescopes. The nature of the dark  
289 matter is not known but its constituents must be very stable to remain since the Big Bang. The  
290 theory of the supersymmetry which is unifying fundamental particles and mediators predicts  
291 many of new heavy particles and the lightest supersymmetric particle, the neutralino, is a good  
292 candidate for dark matter.  
293

294 One more open question is the reason for the matter/antimatter asymmetry. Matter and  
295 antimatter should have been created in the same amount at the moment of the Big Bang. Most  
296 of it has annihilated but because of asymmetry, there was more matter than antimatter which  
297 led to the state of the Universe we observe now. There is a phenomenon of the CP-violation  
298 in weak interactions observed and described which predicts the asymmetry at a certain level.  
299 However, the effect of the CP-violation is not large enough to account for the observed amount  
300 of the matter and, therefore, the total matter/antimatter asymmetry remains unexplained.  
301

302 The measurement of the photon transverse momentum spectrum ( $P_T^\gamma$ ) of the  $W\gamma$  process has  
303 a goal to both test the SM and search for the BSM physics. The low  $P_T^\gamma$  region is not expected  
304 to be affected by any new physics and must agree well with the SM predictions while the high  
305  $P_T^\gamma$  region may indicate an existence of new physics if there is an enhancement over the SM  
306 predictions. The excess would be indirect evidence of the BSM particles like supersymmetric  
307 particles or additional gauge bosons which could be part of the explanation of the dark matter  
308 presence or difference in magnitudes of different interactions. More theoretical details about the  
309 SM description of  $W\gamma$  process as well as possible BSM physics are given in Ch. 2.  
310

<sub>312</sub> **2 W $\gamma$  Production Theory and Former Experimental Re-**

<sub>313</sub> **sults**

<sub>314</sub> Chapter 2 provides deeper theoretical background for the measurement of this dissertation and  
<sub>315</sub> discusses former experimental results. The derivation of the electroweak Lagrangian is described  
<sub>316</sub> in Ch. 2.1, including the appearance of TGC and QGC terms. Then concepts of the cross section  
<sub>317</sub> and the luminosity are discussed in Ch. ???. More specific details regarding the SM cross section  
<sub>318</sub> of W $\gamma$  are summarized in Ch. ???. Possible causes and potential effects of aTGC are explained in  
<sub>319</sub> Ch. 2.4. Finally, Ch. ?? lists former physics experiments which probed the same aTGC vertex  
<sub>320</sub> which is probed in the measurement of this dissertation including measurements of exactly the  
<sub>321</sub> same process at lower LHC beam energy.

<sub>322</sub>

## 323 2.1 Electroweak Theory of the Standard Model

324 To develop a quantum field theory, we start with the Lagrangian of free fermions. In order  
325 to describe a system with a conservation of a physical quantity, the Lagrangian is required to  
326 satisfy a local invariance with respect to a certain transformation. For instance, a conservation  
327 of an electric charge requires a local invariance under  $U(1)$  transformation for the QED La-  
328 grangian [7]. The requirement of the local invariance introduces an interaction of a new vector  
329 field (or several fields) with our free fermions. The new vector field is a mediator of an inter-  
330 action conserving the physical quantity. To provide a full description for a new boson field, in  
331 addition to the interaction term we introduce an invariant term for the kinetic energy of the bo-  
332 son. Such approach allows us to derive the Lagrangian which is locally invariant with respect to  
333 a certain gauge transformation and contains interacting fermions as well as interaction mediators.  
334

335 The SM is a quantum field theory invariant under the local  $SU(3)_C \times SU(2)_L \times U(1)_Y$  trans-  
336 formation [7]. The SM Lagrangian includes all observed quantum fields and their interactions.  
337

338 The part of the SM Lagrangian based on the  $SU(3)_C$  symmetry and is called QCD or theory  
339 of strong interactions. QCD has three types of charges which are called colors: red, blue, and  
340 green. To be a subject of strong interaction, a fermion must posses a color charge. Quarks  
341 and antiquarks are such fermions. The requirement to satisfy the gauge invariance with respect  
342 to  $SU(3)_C$  transformations generates eight massless gluons, and the non-abelian nature of the  
343  $SU(3)$  group generates self-interactions of gluons including three-gluon and four-gluon vertices.  
344

345 The part of the SM Lagrangian based on the  $SU(2)_L \times U(1)_Y$  symmetry is a foundation of the  
346 unified theory of electroweak interactions.  $SU(2)_L$  reflects transformations in the weak isospin  
347 space of left-handed fermions ([1], Ch. 9) while  $U(1)_Y$  reflects transformations in a weak hyper-  
348 charge space of all fermions. The requirement of the local gauge invariant generates four massless  
349 vector bosons which are mediators of electromagnetic and weak interactions. The non-abelian  
350 structure of  $SU(2)$  group generates gauge boson self-couplings the same way as self-interactions  
351 of gluons appear in QCD.  
352

353 Mass terms for the vector bosons would violate the gauge invariance of the electroweak La-  
354 grangian, however it is experimentally known that mediators of weak interactions are heavy  
355 particles with masses  $M_W = 80$  GeV and  $M_Z = 91$  GeV. A possible solution of the discrepancy  
356 is a mechanism of the spontaneous symmetry breaking. QED symmetry group  $U(1)$  remains  
357 unbroken because a photon is massless.  
358

359 The mechanism of the Spontaneous Symmetry Breaking and the appearance of the mass  
360 terms for  $W$  and  $Z$  boson is realized by introducing an additional doublet of scalar fields. After  
361 that, the Lagrangian is being transformed in such a way that  $W$  and  $Z$  bosons acquire masses  
362 through their interactions with a new particle: a Higgs boson ( $H$ ). A photon does not couple to  
363 the Higgs boson remaining a massless particle.  
364

365 The measurement in this dissertation provides a test for the electroweak sector of the SM. We  
366 will retrace the steps of the derivation of the EWK part of the SM Lagrangian starting from terms  
367 of free fermions. The resulting Lagrangian accommodates electroweak gauge bosons including  
368 their self-couplings. One of these self-couplings,  $WW\gamma$ , is the primary focus of our measurement.  
369

370 It is experimentally known that dynamics of weak interactions depends on particle's chiral-  
371 ity ([1], Ch. 4.4.1). In particular, a  $W$  boson couples to left-handed fermions and right-handed  
372 antifermions only. Given different properties of left-handed and right-handed fermions, they  
373 are treated differently by the electroweak theory.  $SU(2)$  doublets are introduced for the wave  
374 functions of left-handed fermions while  $SU(2)$  singlets are introduced for the wave functions of  
375 right-handed fermions. Equations 3 and 4 show wave functions for the first generation fermions.  
376 Wave functions for the other two generations are constructed the same way.  
377

$$\psi_1(x) = \begin{pmatrix} u \\ d' \end{pmatrix}_L, \psi_2(x) = u_R, \psi_3(x) = d'_R. \quad (3)$$

$$\psi_1(x) = \begin{pmatrix} \nu_e \\ e^- \end{pmatrix}_L, \psi_2(x) = \nu_{eR}, \psi_3(x) = e^-_R. \quad (4)$$

The state  $d'$  in Eq. 3 is a weak eigenstate which is a linear combination of mass eigenstates  $d, c$  and  $b$  quark's wave functions and is determined by the quark mixing matrix which is also called Cabibbo-Kobayashi-Maskawa matrix [7]:

381

$$\begin{pmatrix} d' \\ c' \\ b' \end{pmatrix} = V \begin{pmatrix} d \\ c \\ b \end{pmatrix} \quad (5)$$

To derive the unified electroweak Lagrangian, we start with the free fermion terms:

383

$$L_0 = \sum_{j=1}^3 i\bar{\psi}_j(x)\gamma^\mu\partial_\mu\psi_j(x), \quad (6)$$

where  $\gamma^\mu$  are Dirac matrices ([1], Ch. 7.1) and  $\psi_j(x)$  are wave functions determined by Eqs. 3 and 4.

385

The wave function  $\psi_1$  changes under the  $SU(2)_L \times U(1)_Y$  transformations in the following way:

388

$$\psi_1(x) \rightarrow e^{iy_1\beta}U_L\psi_1(x), \quad (7)$$

while the wave functions  $\psi_{(2,3)}(x)$  are singlets of  $SU(2)_L$  and are affected only by  $U(1)$  transformations:

391

$$\psi_{(2,3)}(x) \rightarrow e^{iy_{(2,3)}\beta}\psi_{(2,3)}(x). \quad (8)$$

The transformation in the weak isospin space is defined as  $U_L \equiv e^{i\sigma_i\alpha_i/2}$  where  $\sigma_i$  are Pauli matrices ([1], Ch. 4.2.2). Phases  $\alpha_i(x)$  and  $\beta(x)$  in Eqs. 7 and 8 are arbitrary functions of  $x$ , and  $y_{(1,2,3)}$  are weak hypercharges which are named analogous to electric charges in QED.

395

In order to satisfy the local  $SU(2)_L \times U(1)_Y$  invariance, partial derivatives in Eq. 6 have to be substituted with covariant derivatives:

398

$$D_\mu\psi_1(x) = [\partial_\mu - ig\tilde{W}_\mu(x) - ig'y_1B_\mu(x)]\psi_1(x) \quad (9)$$

$$D_\mu\psi_{(2,3)}(x) = [\partial_\mu - ig'y_{(2,3)}B_\mu(x)]\psi_{(2,3)}(x) \quad (10)$$

where  $g, g'$  are arbitrary constants,

400

$$\tilde{W}_\mu(x) \equiv \frac{\sigma_i}{2}W_\mu^i(x) = \frac{1}{\sqrt{2}} \begin{pmatrix} \sqrt{2}W_\mu^3 & (W_\mu^1 - iW_\mu^2)/\sqrt{2} \\ ((W_\mu^1 + iW_\mu^2)/\sqrt{2}) & -W_\mu^3 \end{pmatrix}, \quad (11)$$

$B_\mu, W_\mu^1, W_\mu^2, W_\mu^3$  are four vector bosons that arise from the requirement of the Lagrangian to be invariant under local  $SU(2)_L \times U(1)$  transformations.

403

The Lagrangian becomes:

405

$$L_0 \rightarrow L = \sum_{j=1}^3 i\bar{\psi}_j(x)\gamma^\mu D_\mu \psi_j(x) \quad (12)$$

406 To make new vector bosons physical fields it is necessary to add terms for their kinetic energies:  
407

$$L_{KIN} = -\frac{1}{4}B_{\mu\nu}B^{\mu\nu} - \frac{1}{4}W_{\mu\nu}^i W_i^{\mu\nu} \quad (13)$$

408 where  $B_{\mu\nu} \equiv \partial_\mu B_\nu - \partial_\nu B_\mu$ ,  $W_{\mu\nu}^i \equiv \partial_\mu W_\nu^i - \partial_\nu W_\mu^i + g\epsilon^{ijk}W_\mu^j W_\nu^k$

409 Off-diagonal terms of  $\tilde{W}_\mu$  are wave functions of charged vector bosons  $W^\pm = (W_\mu^1 \mp iW_\mu^2)/\sqrt{2}$   
410 while  $W_\mu^3$  and  $B_\mu$  are neutral fields which are mixtures of a  $Z$  boson and a photon determined by:  
412

$$\begin{pmatrix} W_\mu^3 \\ B_\mu \end{pmatrix} \equiv \begin{pmatrix} \cos\theta_W & \sin\theta_W \\ -\sin\theta_W & \cos\theta_W \end{pmatrix} \begin{pmatrix} Z_\mu \\ A_\mu \end{pmatrix} \quad (14)$$

413 where  $\theta_W$  is an electroweak mixing angle,  $A_\mu$  is a photon field.

414 In order to be consistent with QED, terms involving  $A_\mu$  in the electroweak Lagrangian must  
415 be equal to the corresponding terms in QED Lagrangian [7]:  
417

$$L_{QED} = i\bar{\psi}(x)\gamma^\mu \partial_\mu \psi(x) - m\bar{\psi}(x)\psi(x) + qA_\mu(x)\bar{\psi}(x)\gamma^\mu \psi(x) - \frac{1}{4}F_{\mu\nu}(x)F^{\mu\nu}(x), \quad (15)$$

418 where  $q$  is electric charge of  $\psi(x)$  field,  $F_{\mu\nu} \equiv \partial_\mu A_\nu - \partial_\nu A_\mu$ .

419 This requirement relates  $g$ ,  $g'$ ,  $\theta_W$  and  $e$  as  $g \sin\theta_W = g' \cos\theta_W = e$  and provides expression  
420 for weak hypercharges:  $y = q - t_3$ , where  $q$  is the electric charge and  $t_3$  is a  $z$ -component of the  
421 weak isospin. This results in  $y_1 = 1/6$ ,  $y_2 = 2/3$ , and  $y_3 = -1/3$  for quarks and  $y_1 = -1/2$ ,  
423  $y_2 = 0$ , and  $y_3 = -1$  for leptons. A right-handed neutrino has a weak hypercharge of  $y_2 = 0$ . It  
424 also does not have an electric charge and, as a right-handed fermion, has  $t_3 = 0$  and, therefore,  
425 does not couple to a  $W$  boson. Thus, a right-handed neutrino does not participate in any SM  
426 interaction.

427 Writing  $\tilde{W}_\mu$  in Eq. 13 explicitly, we obtain triple gauge coupling (TGC) and quartic gauge  
428 coupling (QGC) coupling terms:  
430

$$L_{TGC} = -\frac{g}{4}(\partial_\mu W_\nu^i - \partial_\nu W_\mu^i)\epsilon^{ijk}W^{\mu j}W^{\nu k} - \frac{g}{4}\epsilon^{ijk}W_\mu^j W_\nu^k(\partial^\mu W^{\nu i} - \partial^\nu W^{\mu i}) \quad (16)$$

$$L_{QGC} = -\frac{g^2}{4}\epsilon^{ijk}\epsilon^{ilm}W_\mu^j W_\nu^k W^{\mu l}W^{\nu m} \quad (17)$$

431 Substituting  $W_\mu^i$  and  $B_\mu$  in Eq. 16 and Eq. 17 with the wave functions of  $W^\pm$ ,  $Z$  and a photon:  
432

$$B_\mu = -\sin\theta_W Z_\mu + \cos\theta_W A_\mu, \quad W_\mu^3 = \cos\theta_W Z_\mu + \sin\theta_W A_\mu, \quad (18)$$

$$W_\mu^1 = \sqrt{2}(W^+ + W^-), \quad W_\mu^2 = \sqrt{2}(W^- + W^+), \quad (19)$$

433 we receive charged TGC and QGC Lagrangians in the forms of Eqs. 20 and 23.

434  
435 Equation 20 involves  $WWZ$  (Eq. 21) and  $WW\gamma$  (Eq. 22) interactions:  
436

$$L_{TGC} = L_{TGC}^{(1)} + L_{TGC}^{(2)}, \quad (20)$$

$$L_{TGC}^{(1)} = -ie \cot \theta_W (W^{-\mu\nu} W_\mu^+ Z_\nu - W^{+\mu\nu} W_\mu^- Z_\nu + W_\mu^- W_\nu^+ Z^{\mu\nu}), \quad (21)$$

$$L_{TGC}^{(2)} = -ie (W^{-\mu\nu} W_\mu^+ A_\nu - W^{+\mu\nu} W_\mu^- A_\nu + W_\mu^- W_\nu^+ A^{\mu\nu}). \quad (22)$$

437      Equation 23 involves  $WWWW$  (Eq. 24),  $WWZZ$  (Eq. 25),  $WWZ\gamma$  (Eq. 26), and  $WW\gamma\gamma$   
 438      (Eq. 27) interactions:

439

$$L_{QGC} = L_{QGC}^{(1)} + L_{QGC}^{(2)} + L_{QGC}^{(3)} + L_{QGC}^{(4)}, \quad (23)$$

$$L_{QGC}^{(1)} = -\frac{e^2}{2 \sin^2 \theta_W} (W_\mu^+ W^{-\mu} W_\nu^+ W^{-\nu} - W_\mu^+ W^{\mu+} W_\nu^- W^{-\nu}), \quad (24)$$

$$L_{QGC}^{(2)} = -e^2 \cot^2 \theta_W (W_\mu^+ W^{-\mu} Z_\nu Z^\nu - W_\mu^+ Z^\mu W_\nu^- Z^\nu), \quad (25)$$

$$L_{QGC}^{(3)} = -e^2 \cot \theta_W (2W_\mu^+ W^{-\mu} Z_\nu A^\nu - W_\mu^+ Z^\mu W_\nu^- A^\nu - W_\mu^+ A^\mu W_\nu^- Z^\nu), \quad (26)$$

$$L_{QGC}^{(4)} = -e^2 (W_\mu^+ W^{-\mu} A_\nu A^\nu - W_\mu^+ A^\mu W_\nu^- A^\nu). \quad (27)$$

440      In the measurement of this dissertation we probe  $WW\gamma$  coupling (Eq. 22).

441

442      The unified electroweak Lagrangian discussed above involves kinetic energy terms for fermions  
 443      and gauge bosons as well as interactions of fermions with gauge bosons, TGC, and QGC. How-  
 444      ever, this Lagrangian does not contain any mass terms. Because left-handed and right-handed  
 445      wave functions transform differently under the electroweak symmetry, adding fermion mass terms  
 446      of  $\frac{1}{2}m_f^2 \bar{\psi}\psi$  would violate the Lagrangian invariance and, therefore, fermion mass terms are for-  
 447      bidden by the  $SU(2) \times U(1)$  symmetry requirement. Mass terms for gauge bosons also would  
 448      violate the Lagrangian invariance just as a photon mass term  $\frac{1}{2}m^2 A^\mu A_\mu$  would violate  $U(1)$   
 449      invariance of  $L_{QED}$  [1]. Therefore, Lagrangian  $L$  in Eq. 12 contains massless particles only.

450

451      However, it is known from experiments that a  $Z$  boson, a  $W$  boson and fermions are massive  
 452      particles and, therefore, our theory should accommodate their masses. To introduce masses into  
 453      the electroweak Lagrangian, an  $SU(2)_L$  doublet of complex scalar fields  $\phi(x)$  is added to the  
 454      Lagrangian:

455

$$\phi(x) \equiv \begin{pmatrix} \phi^{(+)}(x) \\ \phi^{(0)}(x) \end{pmatrix} \quad (28)$$

456      By selecting a special gauge of  $\phi(x)$  it is possible to spontaneously break electroweak sym-  
 457      metry, generate a new scalar particle, a Higgs boson [7], and introduce mass terms for  $W$  and  
 458       $Z$  bosons and charged fermions through their couplings to the Higgs boson. The strength of the  
 459      coupling constant is proportional to the square of the particle's mass, therefore, heavier particles  
 460      are more likely to interact with  $H$ , and massless particles do not couple to  $H$ .

461

462      The mechanism of generating a fermion's mass involves both left-handed and right-handed  
 463      components of the fermion. If our hypothesis that right-handed neutrinos do not exist is right,  
 464      then the Higgs mechanism does not generate neutrino masses. However, from the experiments  
 465      of neutrino oscillations, neutrinos are known to have masses even though they are orders of  
 466      magnitude smaller than those of other fermions. Several hypotheses were offered to resolve this  
 467      contradiction however at the moment the mechanism of neutrinos to acquire masses remain un-  
 468      known [5].

469

470      In this dissertation, we study an electroweak process  $W\gamma \rightarrow l\nu_l\gamma$ , more specifically, probe  
 471      TGC vertex  $WW\gamma$  (Eq. 22). To do that, we are measuring a differential cross section with

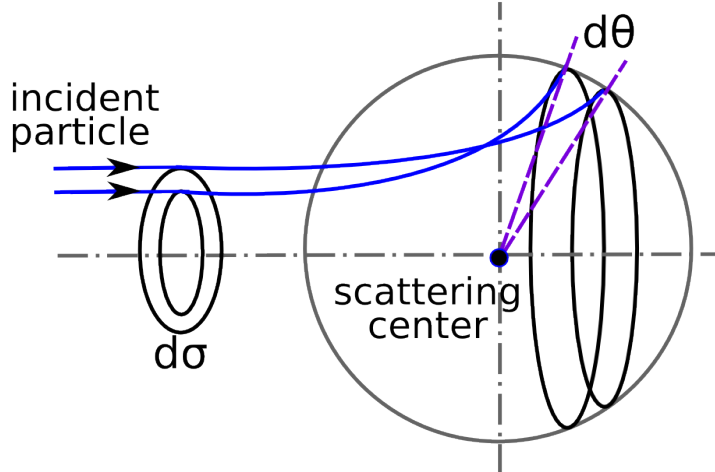
<sup>472</sup> respect to the photon transverse momentum. The concept of the cross section in particle physics  
<sup>473</sup> is discussed in the next chapter.

<sup>474</sup>

## 475 2.2 Cross Section and Luminosity

476 In this dissertation we are measuring the total cross section of the process  $pp \rightarrow l\nu\gamma + X$  and  
 477 its differential cross section in transverse momentum of the photon. A cross section in particle  
 478 physics is an interaction probability per unit flux of incident particles [12]. It can be interpreted  
 479 as an area which must be crossed by an incident particle in order to interact with a scattering  
 480 center, or, in case of a differential cross section, area  $d\sigma$  within which an incident particle must  
 481 appear to be scattered off by an angle  $d\theta$  (Fig. 8). The relationship between  $d\sigma$  and  $d\theta$  gives  
 482 us the expression for a differential cross section  $d\sigma/d\theta$ . Integrating over  $d\theta$ , we obtain the total  
 483 cross section  $\sigma$ .

484 In particle physics we measure a differential cross section with respect to a parameter  $X$   
 485 which can be a parameter of one of final state particles or of a system of final state particles.  
 486 For example, a transverse momentum of a final state photon  $P_T^\gamma$ , an invariant mass of two final  
 487 state leptons  $m_{ll}$ , a number of jets associated with the process  $N_{jets}$  and other parameters.



488 Figure 8: Illustration of the differential cross section concept in the classical case.

490 Referring to the Fig. 8, the number of particles passing through the area  $\sigma$  per unit time is  
 491  $N = L \cdot \sigma$ , where  $L$  is the flux of incident particles and is called luminosity. Therefore, the cross  
 492 section  $\sigma$  of a specific process can be determined from an experiment as  $\sigma = N/L$ .

493 A cross section also can be computed theoretically. The formula to compute a cross section  
 494 is  
 495

$$496 \quad \sigma = \frac{W_{fi}}{L} N_{fs}, \quad (29)$$

497 where  $W_{fi}$  is a transition probability between final and initial states of the system per unit volume,  
 498  $L$  is the flux of initial particles, and  $N_{fs}$  is the density of final states [8], chapter 4.3.

499 500 The formula of the cross section of scattering of two particles to three final state particles  
 501  $1 + 2 \rightarrow 3 + 4 + 5$  is determined by the Fermi's Golden Rule [1]:

$$\sigma = \frac{1}{4\sqrt{(p_1 p_2)^2 - (m_1 m_2)^2}} \int |M|^2 (2\pi)^4 \delta^4(p_1 + p_2 - p_3 - p_4 - p_5) \prod_{j=3}^5 \frac{1}{2\sqrt{\bar{p}_j^2 + m_j^2}} \frac{d^3 \bar{p}_j}{(2\pi)^3}, \quad (30)$$

503 where  $p_i$  are four-momenta and  $\bar{p}_i$  are three momenta of the initial state and the final state  
 504 particles,  $m_i$  are masses of particles,  $M$  is the process amplitude determined by the dynamics  
 505 of the particles interaction. All available momenta of the final state particles is called the phase  
 506 space.

507

508 During proton-proton collisions, at high energy the hard scattering process occurs between  
 509 partons in the protons, as discussed in Ch. 1.4. Therefore, the cross section of a process  
 510  $pp \rightarrow X + Y$  has two ingredients: PDFs and a partonic cross section  $\sigma_{ab \rightarrow X}$ . The partonic  
 511 cross section is described by perturbative QCD while PDFs require non-perturbative computa-  
 512 tions and are determined, in part, from experiments (Fig. 7). According to the QCD factorization  
 513 theorem [9]:

514

$$\sigma(pp \rightarrow X + Y) = \sum_{a,b} \int dx_a dx_b f_a(x_a, Q^2) f_b(x_b, Q^2) \sigma(ab \rightarrow X). \quad (31)$$

515 In the case of  $W\gamma$  process,  $X$  is  $l\nu\gamma$ ,  $ab$  are  $q_i\bar{q}_j$  or  $q_j\bar{q}_i$ .  $Q^2$  is the large momentum scale  
 516 that characterizes hard scattering,  $f_a$  and  $f_b$  are PDFs,  $x_a$  and  $x_b$  are fractions of momenta of  
 517 the partons. In the next sections we will discuss the computation of partonic cross sections of  
 518 the  $W\gamma$  process and possible BSM effects.

519

### 2.3 Standard Model $W\gamma$ Production

A  $W$  boson in proton-proton collisions can be produced in the processes  $q\bar{q}' \rightarrow W$  where  $q$  and  $\bar{q}'$  are a quark and an antiquark which have a total charge of +1 if producing a  $W^+$  boson or -1 if producing a  $W^-$  boson. The processes  $u\bar{d} \rightarrow W^+$  and  $d\bar{u} \rightarrow W^-$  are the most likely to occur because  $u$  and  $d$  are valence quarks in a proton. There are twice as many  $u$  quarks in a proton as  $d$  quarks, therefore,  $W^+$  is produced twice more frequently than  $W^-$ . Antiquarks  $\bar{d}$  and  $\bar{u}$  come from sea  $q\bar{q}$  pairs of the other proton.

One created, a  $W$  boson decays immediately and in an experiment one detects its decay products rather than the  $W$  boson itself. Decay modes of a  $W$  boson include  $W^\pm \rightarrow l^\pm \nu_l (\bar{\nu}_l)$  where  $l^\pm = e^\pm, \mu^\pm$  or  $\tau^\pm$  with branching fractions of 11% per a leptonic channel [5]. The remaining 67% account for various  $W \rightarrow q\bar{q}'$  decays. In this dissertation we only consider  $W^\pm \rightarrow \mu^\pm \nu_\mu (\bar{\nu}_\mu)$  and  $W^\pm \rightarrow e^\pm \nu_e (\bar{\nu}_e)$  channels.

A photon can be emitted from any charged particle of the process: a quark, an antiquark, a charged lepton or a  $W$  boson (Fig. 9, top). A quark and an antiquark are initial state particles and, therefore, if one of them radiates a photon, we call such process the initial state radiation (ISR). A muon or an electron is a final state particle and if it radiates a photon, we call such process the final state radiation (FSR). Finally, a  $W$  boson is a gauge boson and if it radiates a photon, the process has a vertex with three gauge bosons:  $WW\gamma$ , and we call such process the triple gauge coupling (TGC). We cannot distinguish between these processes experimentally because we detect final state particles only.

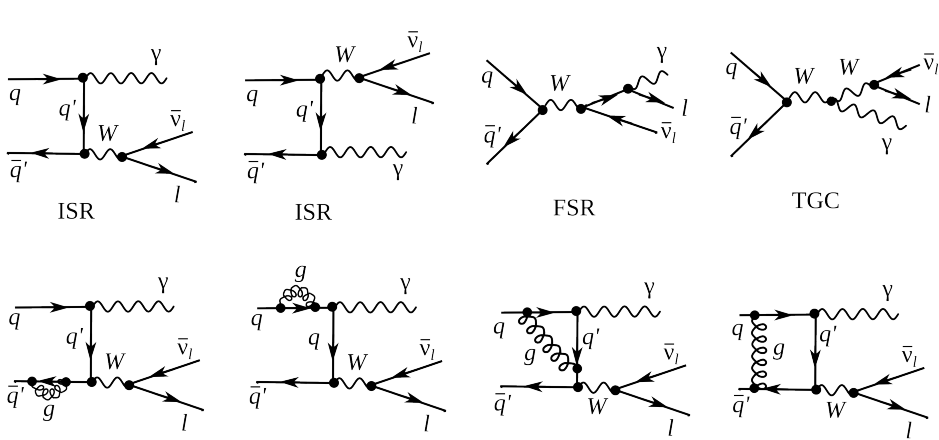


Figure 9: Feynman diagrams of  $W\gamma$  production. Top: LO diagrams, bottom: several examples of NLO in QCD.

The electroweak Lagrangian is described in Chapter 2.1. It is possible to derive equations of motion from the Lagrangian for any fields involved [1]. However, in a quantum field theory equations of motion cannot be solved exactly and, therefore, the perturbative approach is used if a coupling constants is  $g \ll 1$ .

To represent the process graphically Feynman diagrams were invented. Also the diagrams can be used to calculate the process amplitude  $M$  from Eq. 30 because they are determined by Lagrangian terms relevant to the process. There is infinite number of Feynman diagrams corresponding to any specific process and the total amplitude of the process is a sum of individual amplitudes of each diagram and it is not technically possible to take into account all of them. Each vertex introduces a factor in the amplitude of the process that is proportional to

554 the coupling constant. If the coupling constant is  $g \ll 1$ , the perturbative approach arranges  
555 all the diagrams by orders of contribution, and, therefore, the Feynman diagrams with fewer  
556 vertices would give a significantly larger contribution to the amplitude. In Fig. 9 examples of  
557 the Leading Order (LO) and the Next-to-Leading Order (NLO) Feynman diagrams are shown  
558 (top and bottom diagrams respectively).

559

560 At LO, the  $W\gamma$  process is represented by four Feynman diagrams including one FSR, one  
561 TGC and two ISR diagrams. Each LO diagram has three vertices. The first calculation of the  
562  $W\gamma$  process with necessary formulas can be found in [14].

563

564 The NLO corrections to the amplitude of the  $W\gamma$  process that are shown in Fig. 9 are QCD  
565 corrections only, which include gluon loops at the same quark line and exchange of a gluon be-  
566 tween two different quark lines, however, QED and weak NLO diagrams are also possible. QED  
567 corrections involve radiations of extra photons by charged particles, exchange of photons be-  
568 between different charged particles or a photon can be radiated and absorbed by the same charged  
569 particle forming a loop. Similarly, weak corrections involve extra virtual  $W$  or  $Z$  bosons. The  
570 QCD corrections are the largest among the discussed correction types because the QCD coupling  
571 constant is the largest.

572

573 A theoretical cross section in particle physics is important not only for analyzing a mea-  
574 surement result but also for producing a simulation which is then used while performing the  
575 measurement. In a simulation, a large set of  $pp$  collisions resulting in a physics process of in-  
576 terest is modeled creating a data set that mimics real data. A typical simulation consists of  
577 two parts: the generation of the process and the simulation of particles paths through the de-  
578 tector. The first stage contains a collection of events with final state particles with kinematic  
579 quantities distributed according to theoretical predictions for a given process. This stage relies  
580 on the theory including the cross section and also all dynamics of the process. The second stage  
581 simulates the interaction with media during propagation of particles through the model of the  
582 detector as well as the response of detector electronics. In its final form, a simulated dataset has  
583 the same format and content of detector signals for each event as real data, and can undergo the  
584 same reconstruction and analysis procedure as real data would.

585

586 The most precise theoretical  $W\gamma$  cross section available is the Next-to-Next-to-Leading Order  
587 (NNLO) cross section in QCD [15]. The effects of the NNLO correction over the NLO correction  
588 and over the LO result are shown in Fig. 10 for the transverse mass of the final state particles  
589  $m_T^{l\nu\gamma}$  and for the rapidity difference between a charged lepton and a photon  $\Delta_{l\gamma}$ . The NNLO and  
590 NLO theoretical predictions for the photon transverse momentum  $p_T^\gamma$  are overlaid with 7 TeV  
591 ATLAS result. The contribution from higher order corrections is estimated to be  $\pm 4\%$ . However,  
592 the NNLO theoretical result was published only recently, in 2015, and no NNLO  $W\gamma$  simulation  
593 is available at this time. The simulation used in this analysis is LO + up to two hadronic jets  
594 simulation which was found to give the same predictions as the NLO result.

595

596 In addition to the SM predictions, there are certain BSM theories which predict an enhance-  
597 ment of the contribution from the TGC diagram. The discussion of these BSM effects and how  
598 they affect the  $W\gamma$  process takes place in Chapter 2.4.

599

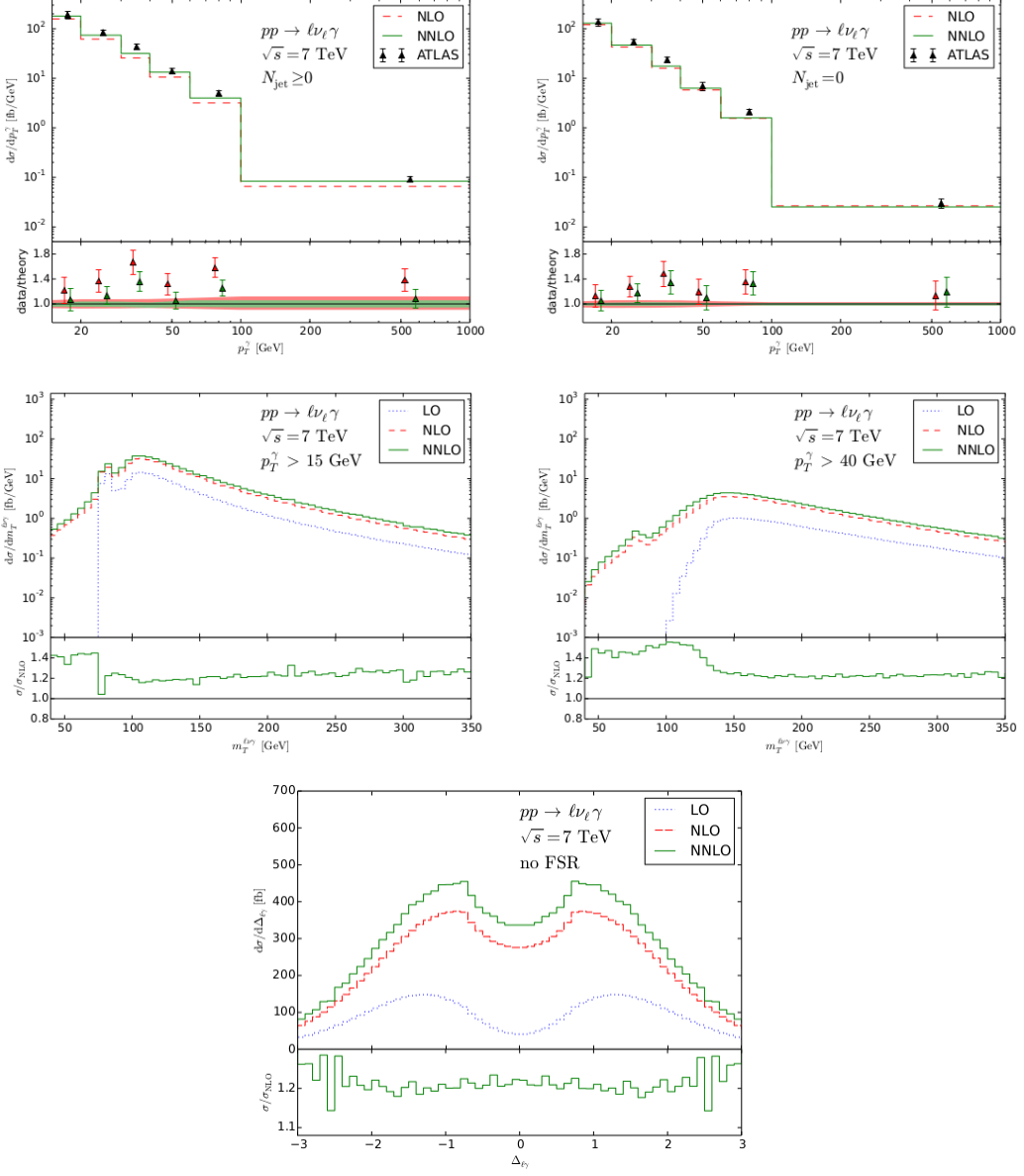


Figure 10: Theory spectra.

## 600 2.4 Anomalous $W\gamma$ Production

601 Most BSM physics theories predict the existence of particles which are heavier than the discov-  
 602 ered energy range. If their masses are not accessible even by the most energetic machines, the  
 603 direct detection of such particles is not possible. However, they can contribute to the productions  
 604 of lower energetic particles as virtual particles. They would give additional contributions to the  
 605 process amplitude and, therefore, there would be more events produced in the process than one  
 606 can expect based on the SM predictions.

607 These effects can be probed by precision measurements of the SM processes. In the elec-  
 608 troweak sector processes of such interest include diboson and triboson productions which can  
 609 occur through triple gauge couplings and quartic gauge couplings.

611 TGC and QGC are represented by vertices with three and four bosons (Fig. 11). As discussed  
 612 in Chapter 2.1, charged TGC and QGC (those that include two or four  $W$  bosons) are possible  
 613 at tree level in the SM while neutral TGC and QGC (those that do not include any  $W$  bosons)  
 614 are not.

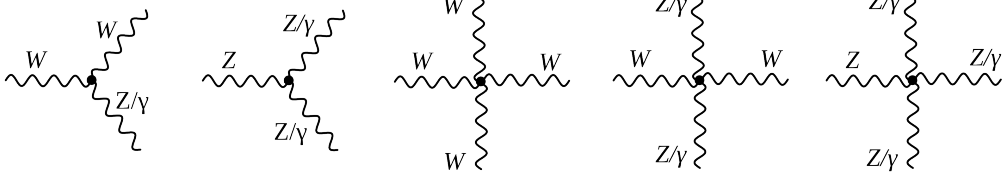


Figure 11: TGC and QGC vertices. The first, third, and fourth vertices are allowed in the SM while the second and the fifth are not.

617 To account for the effects from the potential loops of heavy particles, we introduce an ef-  
 618 fective Lagrangian with arbitrary values of coupling constants which can be shrunk to the SM  
 619 Lagrangian if these constants would have their SM values. Such approach makes our searches  
 620 model-independent because we do not specify which exactly particles form the loops but instead  
 621 just check whether there is a deviation from the SM.

622 In  $W\gamma$  measurement we can probe  $WW\gamma$  vertex only. The most general Lorentz invariant  
 623 Lagrangian of this vertex takes the following form [17]:

$$625 iL_{eff}^{WW\gamma} = iL_{eff(1)}^{WW\gamma} + iL_{eff(2)}^{WW\gamma} + iL_{eff(3)}^{WW\gamma} \quad (32)$$

$$iL_{eff(1)}^{WW\gamma} = e[g_1^\gamma A^\mu (W_{\mu\nu}^- W^{+\nu} - W_{\mu\nu}^+ W^{-\nu}) + \kappa_\gamma W_\mu^+ W_\nu^- A^{\mu\nu} + \frac{\lambda_\gamma}{m_W^2} A^{\mu\nu} W_\nu^{+\rho} W_{\rho\mu}^-] \quad (33)$$

$$iL_{eff(2)}^{WW\gamma} = e[i g_5^\gamma \epsilon_{\mu\nu\rho\sigma} ((\partial^\rho W^{-\mu}) W^{+\nu} - W^{-\mu} (\partial^\rho W^{+\nu})) A^\sigma + i g_4^\gamma W_\mu^- W_\nu^+ (\partial^\mu A^\nu + \partial^\nu A^\mu)] \quad (34)$$

$$iL_{eff(3)}^{WW\gamma} = e[\frac{\tilde{\kappa}_\gamma}{2} W_\mu^- W_\nu^+ \epsilon^{\mu\nu\rho\sigma} A_{\rho\sigma} - \frac{\tilde{\lambda}_\gamma}{2m_W^2} W_{\rho\mu}^- W_\nu^{+\mu} \epsilon^{\nu\rho\alpha\beta} A_{\alpha\beta}] \quad (35)$$

626 where  $e$  is the absolute value of the electron charge,  $A^\mu$  is the photon field,  $W^{\pm\mu}$  are fields of  
 627  $W^\pm$  bosons,  $W_{\mu\nu} = \partial_\mu W_\nu - \partial_\nu W_\mu$ ,  $A_{\mu\nu} = \partial_\mu A_\nu - \partial_\nu A_\mu$ ,  $m_W$  is the mass of a  $W$  boson,  $g_1^\gamma$ ,  $\kappa_\gamma$ ,

628  $\lambda_\gamma$ ,  $g_5^\gamma$ ,  $g_4^\gamma$ ,  $\kappa_\gamma$ , and  $\tilde{\lambda}_\gamma$  are constants.  
 629

630 Despite there are 7 constants in the extended Lagrangian, only  $\lambda_\gamma$  and  $\kappa_\gamma$  are considered  
 631 in the aTGC searches. The rest of the constants are fixed to their SM values based on various  
 632 considerations. Thus,  $g_1^\gamma = 1$  and  $g_5^\gamma = 0$  are fixed to obey the electromagnetic gauge invariance  
 633 for the on-shell photons. The non-zero value of  $g_5^\gamma$  also violates C and P conservations, and  
 634 non-zero values of  $g_4^\gamma$ ,  $\kappa_\gamma$ ,  $\tilde{\lambda}_\gamma$  violate the CP conservation law. Such violation parametrizations  
 635 are not considered in charged TGC measurements now but might get considered in the future.  
 636

637 The presence of aTGC would have larger effects at high energy scales. Fig. 12 shows these  
 638 effect in  $P_T^\gamma$  spectrum of 7 TeV  $W\gamma \rightarrow \mu\nu\gamma$  measurement. It is seen on the plot that aTGC spec-  
 639 trum at low  $P_T^\gamma$  coincides with the SM prediction but for higher  $P_T^\gamma$  the disagreement becomes  
 640 more significant.  
 641

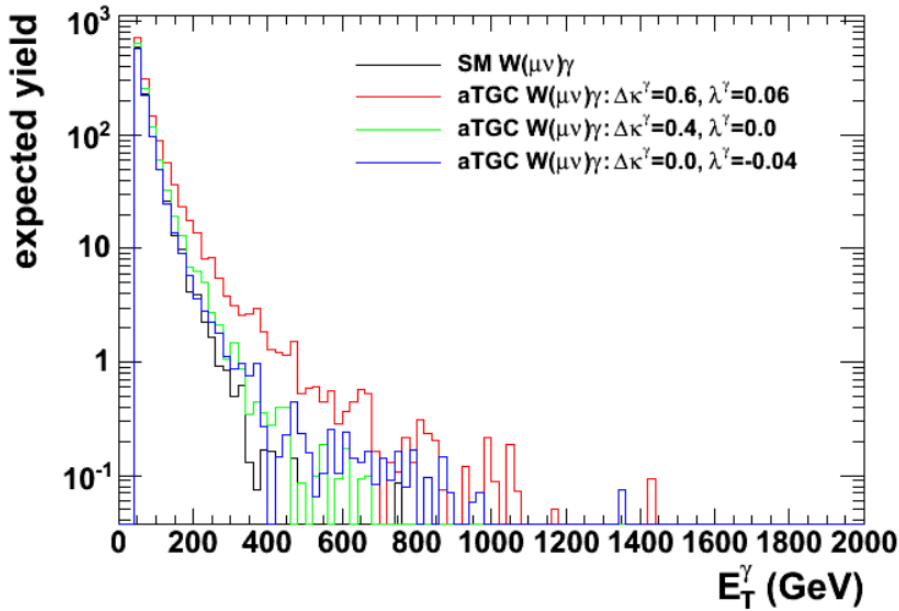


Figure 12: Distributions of  $P_T^\gamma$  of simulated  $W\gamma \rightarrow \mu\nu\gamma$  events with different values of aTGC constants at LHC energy of  $\sqrt{s} = 7$  TeV. Source of figure: [18].

## 642 2.5 Measurements in the Past

643 ATGC parameters of  $WW\gamma$  vertex can be probed in  $W\gamma$ ,  $WW$ , and  $WZ$  measurements. Lim-  
 644 its on  $\Delta\kappa_\gamma$  and  $\lambda_\gamma$  constants from different D0 [19], LEP [20], ATLAS [21], [22], [23] and  
 645 CMS [25], [26], [27], [28] measurements are summarized in Fig. 13.

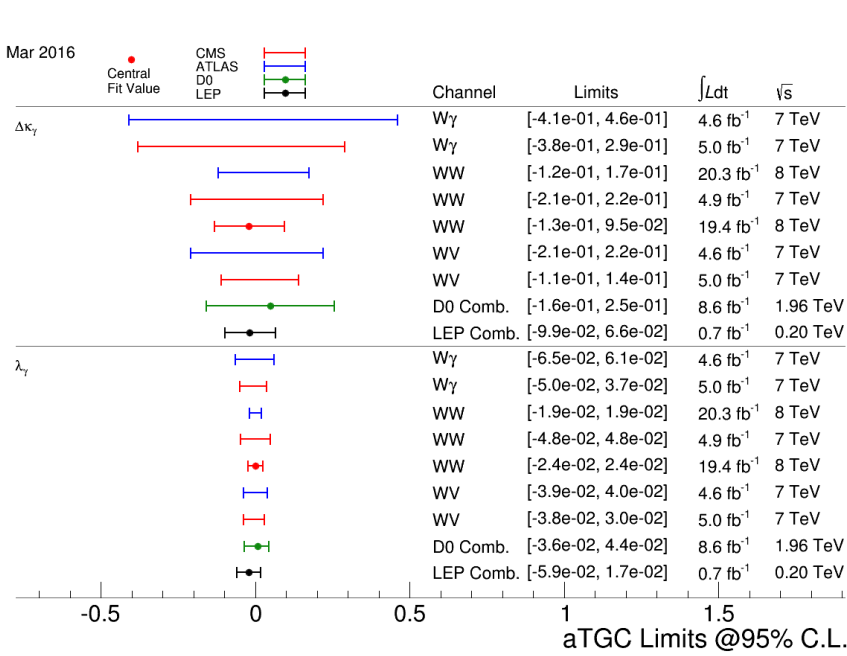


Figure 13: Summary of limits on the  $WW\gamma$  aTGC coupling constants. Figure from [24].

647 The most recent measurements of  $W\gamma$  production were performed by CMS [25] and AT-  
 648 LAS [21] collaborations with  $pp$  collisions at  $\sqrt{s} = 7 \text{ GeV}$  collected in 2011. The measurements  
 649 are based on  $5 \text{ fb}^{-1}$  and  $4.6 \text{ fb}^{-1}$  of integrated luminosity with CMS and ATLAS respectively.  
 650 Both collaborations considered two channels:  $W\gamma \rightarrow \mu\nu\gamma$  and  $W\gamma \rightarrow e\nu\gamma$ .

651 Dibosons processes are rare in  $pp$ -collisions and analysts have to filter out events of their  
 652 interest from many processes which are more likely to happen. To do that, variety of selection  
 653 criteria is applied which reject most of background events increasing a signal fraction in the  
 654 selected sample as much as possible. However, even after all possible selection criteria are ap-  
 655 plied, majority of selected events are still background events and it is not possible to reduce the  
 656 background any further without also significantly reducing signal.

657 The major source of such irreducible background is the fake photon background where  
 658 hadronic jets are misidentified as photons. Such events originate from  $W+\text{jets}$  process mostly  
 659 but  $Z+\text{jets}$  and  $t\bar{t}+\text{jets}$  events contribute to this source of the background as well. The second  
 660 major background for the electron channel is the fake photon background where electron can be  
 661 misidentified as a photon. Such events are coming from  $Z+\text{jets}$  events. Other sources of back-  
 662 grounds include real- $\gamma$  backgrounds, fake lepton + real photon and fake lepton + fake photon  
 663 sources.

664 Both channels provide measurements of  $p_T^\gamma$  spectra because this variable is the most sensitive  
 665 to the potential ATGC. The  $p_T^\gamma$  spectra of the selected events in data superimposed with selected  
 666 events in the simulation of the signal and estimated background contribution for the muon and  
 667 electron channels are shown in Fig. 14 for CMS and in Fig. 15 for ATLAS. Both measurements  
 668 show a good agreement.

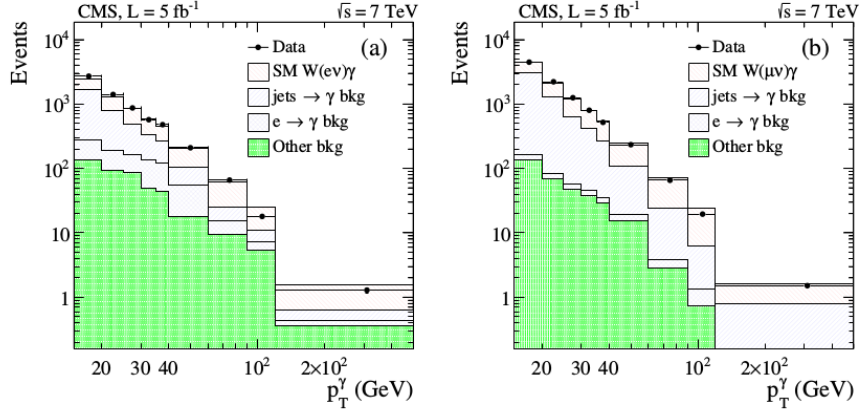


Figure 14: The distribution fo the  $p_T^\gamma$  of  $W\gamma$  candidates in the analysis of 7 TeV CMS data. Data vs signal MC + background estimates. Left:  $W\gamma \rightarrow e\nu\gamma$ , right:  $W\gamma \rightarrow \mu\nu\gamma$  [25].

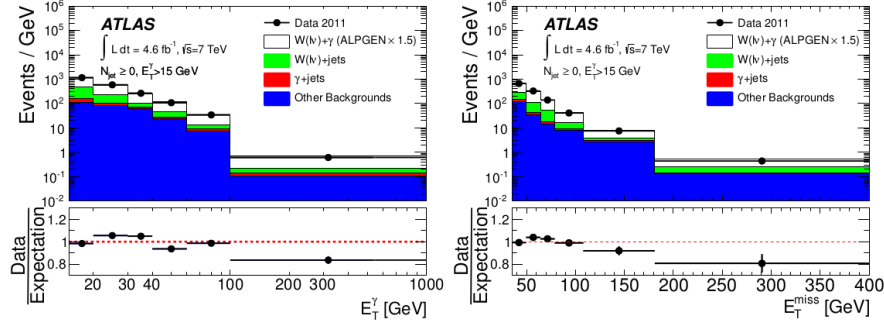


Figure 15: The distribution fo the  $p_T^\gamma$  (left) and  $E_T^\gamma$  (right) of  $W\gamma$  candidates in the analysis of 7 TeV ATLAS data. Data vs signal MC + background estimates [21].

CMS provides measurements of the  $P_T^\gamma$  spectrum, the total cross section within the phase spaces of  $\Delta R > 0.7$ ,  $P_T^\gamma > 15$  GeV,  $P_T^\gamma > 60$  GeV and  $P_T^\gamma > 90$  GeV, and limits on aTGC coupling constants. The phase space restrictions come from the considerations of the detector acceptance, reducing heavily background-dominated regions and theory.

ATLAS, in addition to the  $P_T^\gamma$  spectrum, total cross section and limits, provides the differential cross section and cross section with different number of associated jets. No evidence of a new physics is observed.

In this dissertation we are measuring total and differential  $d\sigma/dP_T^\gamma$  cross section however we do not derive limits on aTGC coupling constants. The measurement details and results are available in Chapter 5.

685

686 **3 Experimental Setup**

### 687 3.1 Large Hadron Collider

688 The Large Hadron Collider (LHC) [31], [32], [33] is the largest particle accelerator and the most  
689 ambitious research facility ever built. The LHC is placed into a tunnel originally built for the LEP  
690 accelerator. The LEP was decommissioned to make room for the LHC. The tunnel is about 27 km  
691 in circumference, located at the Swiss-French boundary up to 100 meters undergroud.

692 Before entering LHC, particle beams are going through several stages of the acceleration and  
693 the LHC is the last element of the chain of the CERN's accelerator complex (Fig. 16). Protons  
694 are extracted from hydrogen atoms, are accelerated by Linac2 to energies of 5 MeV, then injected  
695 into the Proton Synchrotron Booster (PSB) where they reach energies of 1.4 GeV. After that  
696 protons are sent to PS and Super PS (SPS) where they are accelerated up to 25 GeV and 450 GeV  
697 respectively. Finally, protons enter the LHC and are accelerated to reach their collision energies  
698 of several TeV per beam. Besides protons, the complex also accelerates and collides lead ions  
700 however in this dissertation we analyze data from proton-proton collisions only and, therefore,  
701 are not discussing lead ion collisions.

702 Main goals of LHC were to detect the SM Higgs boson if it existed and to search for evidences  
703 of BSM physics which may give a clue on understanding the phenomena including but not limited  
704 to the dark matter, the matter-antimatter asymmetry, the nature of the gravitational force. Six  
705 detectors are installed at the LHC to detect particles and perform the relevant measurements.  
706 There are general purpose detectors ATLAS and CMS, there is LHCb which specializes of the  
707 physics of B-mesons, and ALICE which is designed to detect products of heavy ion collisions. In  
708 addition, there are two relatively small detectros: LHCf and TOTEM which are installed close  
709 to the ATLAS and CMS collision points respectively.

711 A new particle with mass  $m = 125$  GeV was discovered by the CMS [3] and the ATLAS [4]  
712 collaborations in 2012. The particle is consistent with the SM Higgs boson predicted by the  
713 EWK sector of the SM. The discovery of the Higgs boson is the greatest achievement by the  
714 LHC to date.

716 While different BSM searches have been constituting a significant part of the LHC physics  
717 program since the beginning of its operation, no deviations from the SM were found by any of  
718 the experiments. The searches continue with higher beam energies and larger amount of data.

721 The design energy of the LHC is 7 TeV per beam however several lower energy points were  
722 and are being probed. In 2010-2011 the LHC operated at energy of 3.5 TeV per beam which was  
723 already higher than energy of any other collider. In 2012 the energy increased up to 4 GeV. In  
724 2013-2014 the LHC was shut down for upgrades. Collisions were restarted at 6.5 TeV in 2015  
725 and the LHC is still operating at this energy in 2016.

726 All important measurements performed at lower energies are also repeated at higher energies  
727 because the ability to probe higher energy scales increases our chances for a discovery and even  
728 if no deviations from the known physics are found at a given energy point, the discovery is still  
729 possible to happen as we go higher in the energy.

731 In addition to the beam energy, there are many other collider parameters. A brief summary  
732 of them is available in Tab. 2. One of the most important parameters of an accelerator is the  
733 ability to produce a large number of interesting collisions which is determined by the luminosity.  
734 The instantaneous luminosity is determined by the following expression [5]:

736

$$737 L = f \frac{n_1 n_2}{4\pi\sigma_x\sigma_y}$$

738 where  $n_1$  and  $n_2$  are numbers of particles in colliding bunches,  $f$  is a frequency of collisions,  
739  $\sigma_x$  and  $\sigma_y$  are beam sizes in horizontal and vertical directions. To determine the integrated  
740 luminosity, one has to integrate the instantaneous luminosity over time:

$$L_{int} = \int L dt$$

The luminosity of the LHC is also higher than of any previously existed collider. The integrated luminosity of the LHC for different years of the operation are shown in Fig. 17. Run periods of LHC in 2010-2012 refer to Run I of the LHC operation. While working on energy of  $\sqrt{s} = 7$  TeV, LHC delivered  $44.96 \text{ pb}^{-1}$  and  $6.1 \text{ fb}^{-1}$  of data in 2010 and 2011 year respectively. In 2012 the working energy of LHC was  $\sqrt{s} = 8$  TeV, and the integrated luminosity was  $L_{int} = 23.3 \text{ fb}^{-1}$ . After a long shutdown, LHC was upgraded for Run II, to operate on  $\sqrt{s} = 13$  TeV in 2015 and delivered  $4.22 \text{ fb}^{-1}$  of data by the end of 2015. In 2016 LHC continues operation on  $\sqrt{s} = 13$  TeV and by the end of September the integrated luminosity already exceeded a value of  $30 \text{ fb}^{-1}$  [37].

The measurement of this dissertation is performed at the energy of 4 TeV per beam or at the center of mass energy  $\sqrt{s} = 8$  TeV with  $19.6 \text{ fb}^{-1}$  of data. The same process was measured at  $\sqrt{s} = 7$  TeV with about four times less amount of data by both CMS and ATLAS. These measurements are discussed in greater details in Ch. 2.5.

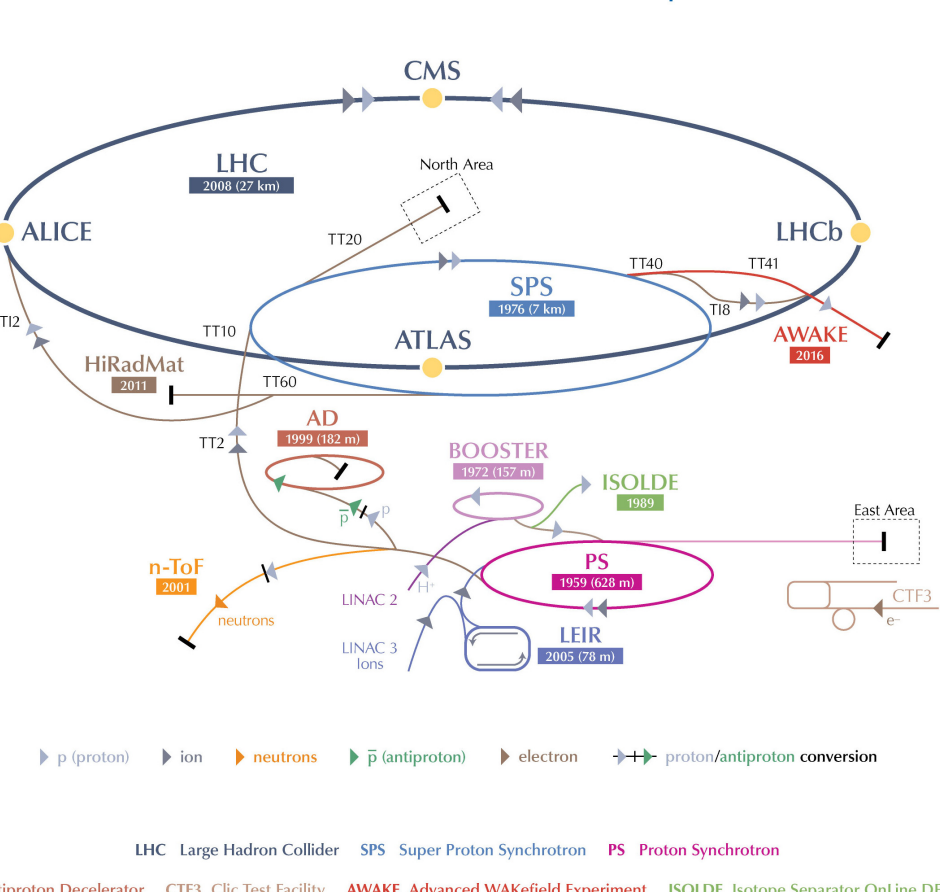


Figure 16: CERN's accelerator complex. Source of the figure: [34].

Table 2: Main parameters of LHC [31]

Circumference	27 km
Dipole operating temperature	1.9 K
Number of magnets	9593
Number of main dipoles	1232
Number of main quadrupoles	392
Number of RF cavities	8 per beam
Nominal energy, protons	7 TeV
Nominal energy, lead ions	2.76 TeV per nucleon
Peak magnetic dipole field	8.33 T
Min. distance between bunches	7 m
Design luminosity	$10^{34} \text{ cm}^{-2} \text{ s}^{-1}$
No. of bunches per proton beam	2808
No. of protons per bunch (at start)	$1.1 \times 10^{11}$
No. of collisions per second	600 millions

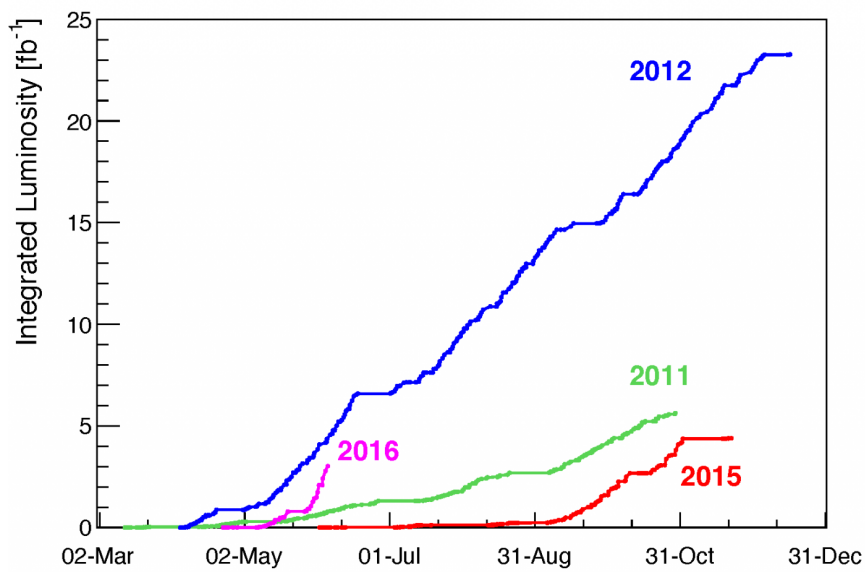


Figure 17: LHC integrated luminosity by year. Source of the figure: [35].

### 3.2 Compact Muon Solenoid

#### 3.2.1 Introduction

The CMS is a general-purpose detector designed for detecting various highly energetic particles which are being produced in pp collisions at the LHC. The CMS has a broad program with goals of direct and indirect searches of the BSM physics including but not limited to supersymmetric particles. Its main feature is a huge magnet to create a magnetic field of 4T to curve charged particles in the tracking system and 2T outside to curve muons in the muon system.

766

The CMS detector is a cylindrically symmetric with a colliding beam as a central axis. Cartesian, cylindrical and spherical coordinates are all used to describe the CMS geometry, depending on the context. The  $x$ -axis of the CMS points towards the center of the LHC while the  $y$ -axis points vertically up. The direction of the  $z$ -axis corresponds to the counterclockwise direction of the LHC beam (Fig. 18, left). Cylindrical coordinates are defined as  $r = \sqrt{x^2 + y^2}$ ,  $\phi = \arctan(y/x)$ . Instead of the polar angle  $\theta$ , it is more convenient to use the pseudorapidity  $\eta = -\ln \tan \theta/2$ . A pseudorapidity changes from  $\eta = -\infty$  to  $\eta = +\infty$  for directions parallel to the beam axis with the value of  $\eta = 0$  for a direction perpendicular to the beamlime. This variable is convenient for measurements because a distribution of a massless particle in  $\eta$  is nearly flat. The acceptance of the CMS in  $\eta$  is limited and varies from  $|\eta| = 2.4$  to  $|\eta| = 5.0$  depending on a subdetector.

778

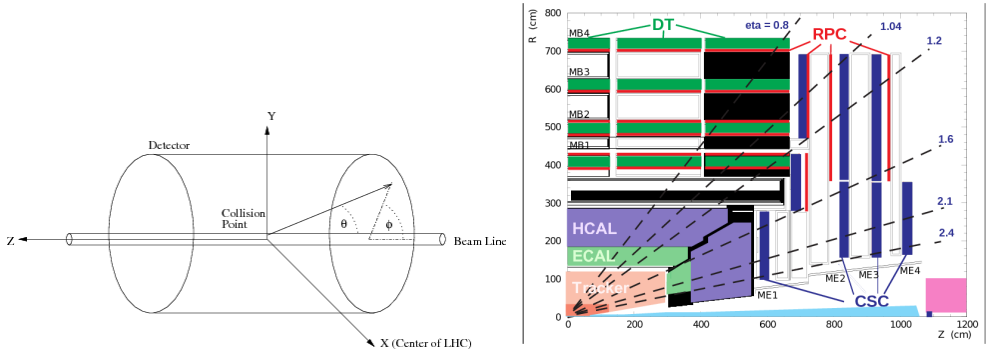


Figure 18: Left: CMS coordinate system. Right: pseudorapidity ranges for different CMS subdetectors.

779

The detector consists, from inner to outer layer, of a tracking system, an electromagnetic calorimeter (ECal), a hadronic calorimeter (HCal), a magnet and a muon system. Having the tracking system, ECal and HCal inside of a large solenoid makes the detector compact. A segment of a CMS slice in  $r - \phi$  plane is shown in Fig. 19.

783

When a heavy particle is produced in a collision, it decays immediately, and we detect its long-living decay products including an electron, a photon, a muon, a neutral hadron or a charged hadron. Depending on the trace left by a particle in different subdetectors we can identify a particle. Electrons and positrons leave curved tracks in the tracking system and then induce showers in the electromagnetic calorimeter (ECal). Photons induce the same electromagnetic showers in ECal however, as neutral particles, they do not leave tracks in the tracking system. Hadrons normally travel through the ECal undisturbed and induce a hadronic shower in the hadronic calorimeter (HCal). Charged and neutral hadrons can be distinguished from each other by checking whether they leave a track in the tracking system or not. Muons are the only particles which penetrate through the ECal, the HCal and the magnet and leave tracks in the CMS muon system. Neutrinos are not detected by CMS.

795

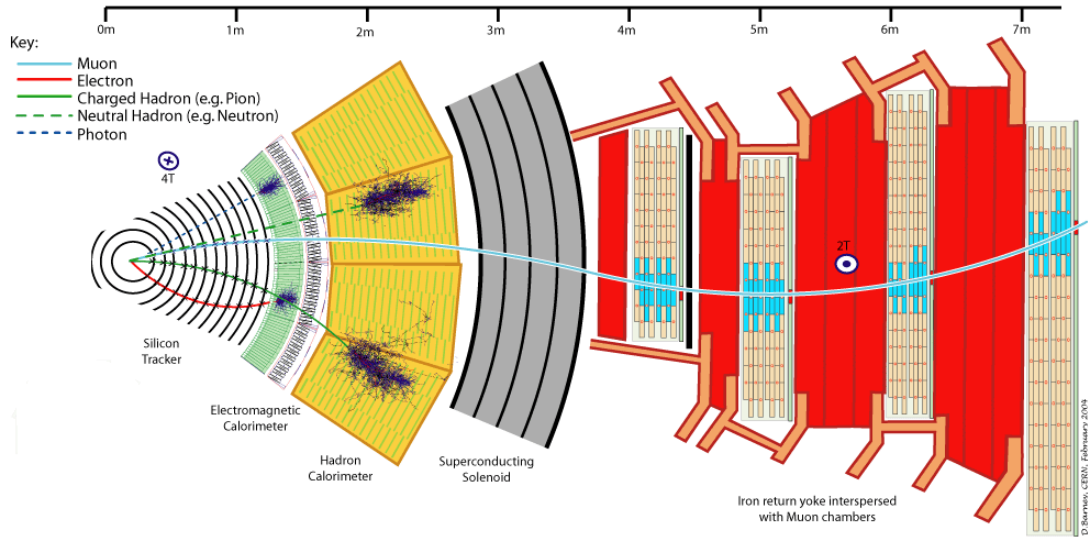


Figure 19: CMS slice.

796 All subdetectors are important for the  $W\gamma$  measurement and the remainder of this chapter  
 797 describes the subdetectors in greater details. Muons and electrons which we have as final state  
 798 particles are both affected by CMS magnetic field allowing the tracking system and the muon  
 799 system to measure their trajectory parameters and momenta. In this dissertation we use the  
 800 information of the primary vertex determined by the tracking system to select our events. Also  
 801 the tracker provide us the information about electrons trajectories and momenta in the electron  
 802 channel and distinguishes between electrons and photons.  
 803

### 804 3.2.2 Magnet

805 A magnetic field in a particle detector is necessary to measure momenta of charged particles  
 806 by track curvatures. The higher the momentum is, the less a particles's path is affected by the  
 807 magnetic field. In CMS it is done in the tracking system for all charged particles and in the  
 808 muon system for muons.  
 809

810 The CMS magnet is placed between layers of HCal and a muon system. It creates a magnetic  
 811 field of 4T inside the magnet, for the tracking system, and 2T outside the magnet, for the muon  
 812 system. It is necessary to have stronger field in the tracking system because a density of tracks  
 813 is much higher there than in the muon system and also the tracking system is much smaller and,  
 814 therefore, more significant curvature is necessary to measure the momentum with high precision.  
 815

816 The magnet is made of superconducting wires. An electric current flowing in the wires creates  
 817 a uniform field inside the solenoid and also provides a magnetic field of a certain configuration  
 818 outside the solenoid.  
 819

### 820 3.2.3 Tracking System

821 The tracking system measures track geometry including particles trajectories and locations of  
 822 primary and secondary vertices and momenta of charged particles. It needs to disturb particles

as little as possible so that they can pass through. Therefore, just a few measurements must be enough to reconstruct the track. The accuracy of a measurement of each hit is  $10 \mu\text{m}$ .

The tracking system consists of silicon pixels and silicon strips (Fig. 20). Collision tracks start at the center and then cross the layers of the tracking system. Tracks are straight in  $r - z$  plane and curved by the magnetic field in the  $r - \phi$  plane. The acceptance of the tracker system in  $r - z$  plane is geometrically limited by  $\eta = 2.5$  ( $\eta = -\ln[\tan \theta/2]$ , where  $\theta$  is a polar angle).

The pixel tracker is the closest subsystem of CMS to the collision point thus it experiences the largest particle flux: at 8 cm from the collision point the flux is about 10 million  $1/(\text{cm}^2\text{s})$ , and the pixel detector with its 65 millions sensors is capable to reconstruct all these tracks. It consists of three layers of cylinders in the barrel with radii of 4 cm, 7 cm and 11 cm and four disks in the endcap, two disks at each side. The tracker is designed in such a way that a single track hits multiple sensors. Then the trajectory is reconstructed based on how much charge is collected on each sensor. This allows us to reach a spacial resolution of 15-20  $\mu\text{m}$  which is much smaller than a distance between sensors.

The strip tracker is placed right after the pixel tracker and occupies the detector volume up to 130 cm around the beam axis. The strip tracker consists of four parts: the tracker inner barrel (TIB), the tracker inner disks (TID), the tracker outer barrel (TOB) and the tracker endcap (TEC) as shown in Fig. 20. In the strip tracker there are over 15,000 sensitive modules with a total number of 10 million strips. Each sensitive module consists of a set of sensors, its support structure and readout elements.

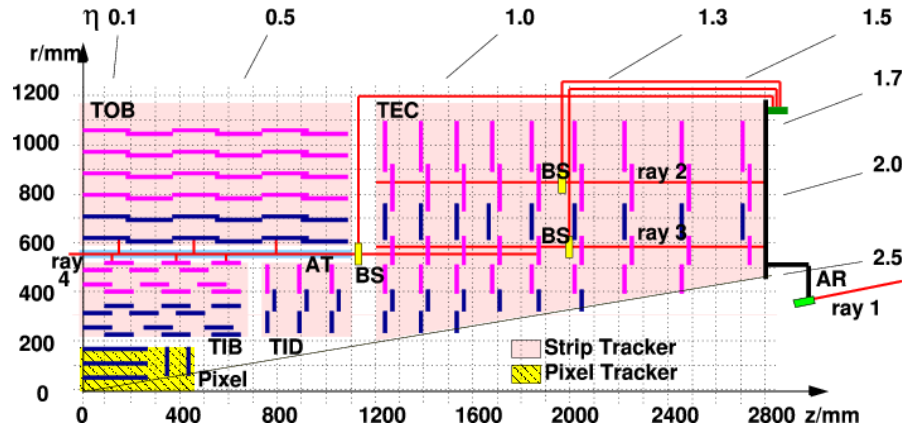


Figure 20: Slice of the CMS tracking system in  $r - z$  plane.

### 3.2.4 Electromagnetic Calorimeter

The ECal measures energy of electrons and photons and also measures geometries of their trajectories. Electrons and photons interact with the ECal substance by inducing electromagnetic showers. Traces left by photons and electrons in the ECal are the same. To distinguish between these two particles, it is necessary to perform matching to the track in the tracking system. If there is a track, then there is an electron (or positron). If there is no track, then the particle is a photon.

The Ecal is a layer between the tracking system and the HCal. It is made of high-density lead tungstate crystals arranged in a barrel section and two endcap sections. The crystals work as scintillators. When electrons and photons pass through it, it produces light proportional to the

858 particle's energy. The scintillated light then is amplified by photomultipliers producing signals  
859 on sensitive elements.

860 It is important for the Ecal to be able to distinguish between high energetic photons and  
861 pairs of lower energetic photons e.g. from a  $\pi^0$  decay. It is especially difficult in the endcap  
862 sections where angle between two photon trajectories is small. Ecal preshower located in front  
863 of the endcaps which have much smaller granularity provide extra spacial precision. Their strips  
864 are 2 mm wide compared to 3 cm wide crystals in the main volume of the ECal.  
865

866

### 867 3.2.5 Hadron Calorimeter

868 The HCal is placed right after the ECal and is the last subdetector within the magnet. The  
869 HCal measures energies of charged and neutral hadrons. In addition, the HCal determines the  
870 track parameters. Match to the tracking system has to be done: if a matching track found, then  
871 it is a charged hadron otherwise it is a neutral hadron.

872

873 The HCal consists of alternate layers of absorbers and scintillators. Hadrons hit brass or steel  
874 plate of absorber producing secondary particles. When emerge into the scintillator, the particles  
875 induce hadronic and electromagnetic showers and emit blue-violet light which is further shifted  
876 to the green region and read out by special boxes within the HCal. The secondary hadrons pro-  
877 duced during the interaction with the absorber interact with the next absorber producing more  
878 showers in the next layers of scintillators and also affect the total energy deposit. All hadrons  
879 must be stopped inside the layers of the HCal.

880

### 881 3.2.6 Muon System

882 Muons pass through the ECal, the HCal and the magnet without interacting. They are the only  
883 particles which are registered in the muon system which is placed outside the magnet and which  
884 is the largest part of CMS detector.

885

886 There are four concentric layers of muon detectors (stations) and iron return yoke between  
887 them. Muons induce several hits in the muon stations which are later fitted and matched to the  
888 tracking system measurements to provide the best possible resolution in the measurements of all  
889 parameters of the muon's trajectory and momentum.

890

891 There are three types of muon chambers used in the CMS muon system: drift tubes (DTs),  
892 cathode strip chambers (CSCs) and resistive plate chambers (RPCs). Overall, there are 1400  
893 muon chambers including 250 DTs, 540 CSCs and 610 RPCs.

894

895 The system of DTs measures positions of muons in the barrel. Each DT chamber is about 2 m  
896 by 2.5 m in size. It consists of 12 layers of aluminium which are grouped by four. There are up  
897 to 60 drift tubes in a layer. The middle group of layers measures  $z$ -coordinate and two other  
898 groups determine the perpendicular coordinate.

899

900 Each drift tube is 4 cm in width, is filled with a gas and has a wire inside. When a charged  
901 particle passes through the volume, it ionizes atoms and the wire receives an electric charge.

902

903 CSCs are placed in endcap regions. CSCs are arrays of anode wires which are crossed by  
904 copper cathode strips placed in a gas volume. When a charged particle penetrates to the gas  
905 volume, it ionizes the gas. Electrons drift to the wires while ions move to the strips. Strips are  
906 perpendicular to wires, thus, we measure two coordinates for each particle.

907

908 RPCs are parallel capacitors made of high-resistivity plastic plates with a space between  
909 them filled with a gas. RPCs provide quick measurements of muon momenta and are used for

910 triggering.

911

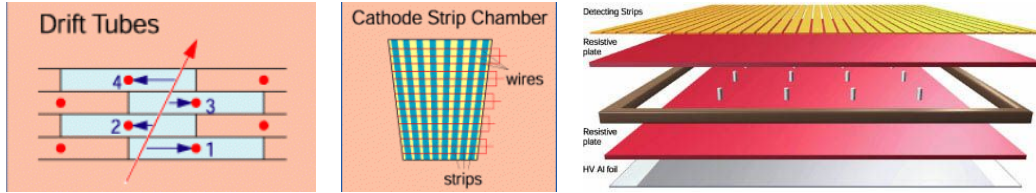


Figure 21: Components of the CMS muon system. Left to right: drift tubes, cathode strip chambers (CSCs), resistive plate chambers (RPCs).

### 912 3.2.7 Triggering and Data Aquisition

913 At peak luminosity, CMS experiences one billion proton-proton collisions per second which come  
914 in bunches separated just by 25 ns from one other. New events come before the events from  
915 the previous bunch crossing left the detector. To process the information from many different  
916 collisions at the same time, data is stored in pipelines.

917

918 It is not technically possible to readout all these events. Moreover, we do not need most  
919 of these events for a physics analysis because most of these events do not have a potential to  
920 discover a new physics. We have resources to store about one hundred events out of one billion  
921 that is why we need a trigger system which quickly decides what the best one hundred events are.

922

923 If the triggers were too loose, and we would select one hundred events too quickly, e.g., out  
924 of a hundred million events, then CMS would not be able to process the rest 90% of events in a  
925 givem set of one billion and we would lose 90% of potentially interesting events.

926

927 If the triggers were too strict, we would select, e.g, ten events out of one billion, not one  
928 hundred and lose CMS potential to store and process data by 90% which would significantly  
929 reduce our chances for a discovery.

930

931 Thus, the challenge of the trigger system is to select the best one hundred events out of one  
932 billion and do that fast to be able to process every single event. To achive this goal, a two-level  
933 trigger system was developed consisting from the Level 1 (L1) trigger and the high level trigger  
934 (HLT) as shown in Fig. 22.

935

936 L1 is a hardware based trigger (Fig. 23). It uses information from the ECal, HCal and muon  
937 system. L1 reduces frequency of coming events from 40 MHz to 100 kHz. Events which did not  
938 pass the L1 trigger are lost forever while events which pass the L1 trigger are temporarily stored  
939 to get checked by the HLT.

940

941 HLT is a software-based trigger. It uses information from all subdetectors and runs quick  
942 reconstruction and identification algorithms to determine types of particles and their kinematics.  
943 It reduces the number of events to 100 Hz. Events which did not pass HLT are lost forever.  
944 Events which pass HLT are arranged into appropriate datasets depending on HLT selection cri-  
945 teria they passed and stored for physics analyses.

946

### 947 3.2.8 Event Reconstruction

948 Where to place particle reconstruction, particle flow algorithm and MET? Check other theses

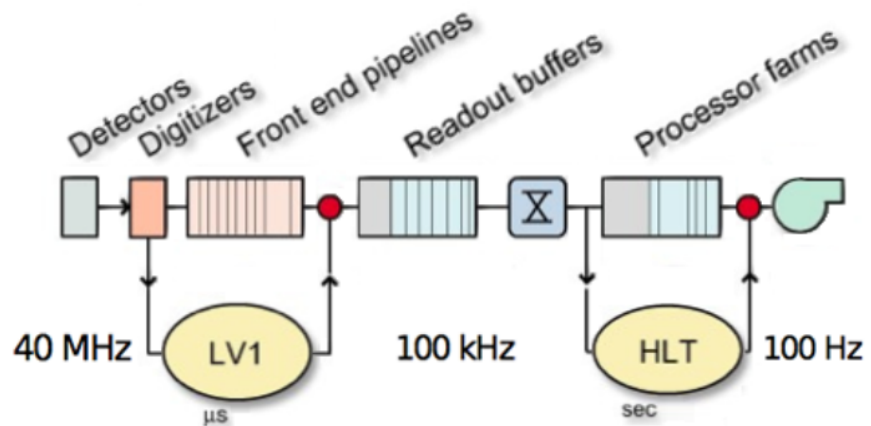


Figure 22: Two-level CMS trigger system.

949        Acceptance: particles which are too collinear and go to pipe; particles which get curved too  
950        strongly

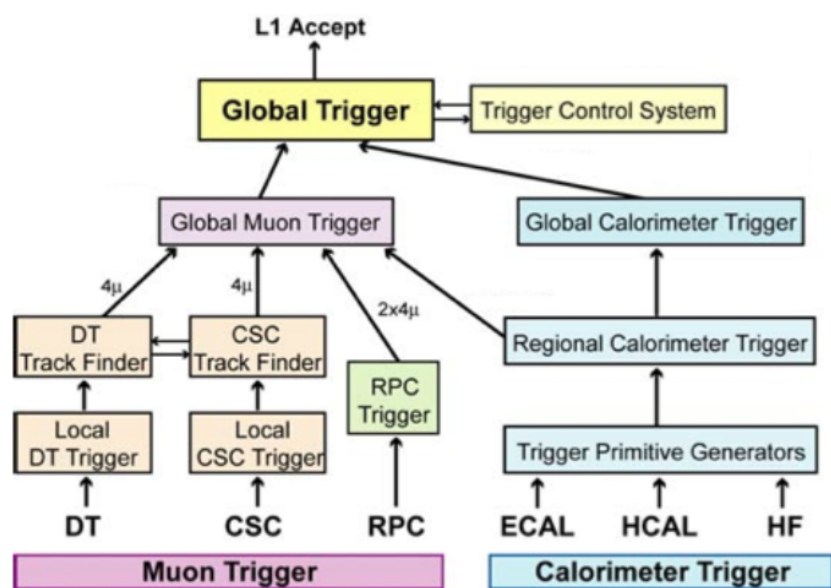


Figure 23: Level 1 CMS trigger system.

951 4 CMS Tracker Alignment

## 4.1 Algorithm

953 Why align?

954 How to align?

955 When align?

956 How to check that your alignment is good?

957 A tracking system detects hits produced by a charged particle traveling through the detector.  
 958 In a presence of a constant magnetic field the particle has a helical trajectory. A reconstruction  
 959 algorithm determines the track parameters by fitting the positions of hits assuming the helix  
 960 trajectory.

961 Better hit resolution and the location uncertainty lead to better precision of a measurement  
 962 of the track parameters. The location uncertainty depends on our knowledge of the positions and  
 963 orientations in space of the tracking system modules. The hit resolution in the CMS pixel detector  
 964 is  $\sim 15 \mu\text{m}$ . When the modules are mounted, their positions are known with precision of  $\sim 200 \mu\text{m}$ .  
 965 Thus, we need to know positions of modules 20 times better than they are known when mounted.

966 The procedure of the determination of the modules locations and orientations is called the  
 967 tracker alignment. The concept of the track-based alignment can be illustrated in the example of  
 968 the alignment of a toy tracker. When a charged particle passing through a detector (Fig. 24, top  
 969 left) it crosses a toy tracker which consists of six flat equidistant modules (Fig. 24, top right). If  
 970 the modules were placed exactly at their designed positions, we would observe the hits exactly at  
 971 the points where the track crosses modules at the points of ideal geometry (Fig. 24, middle left).  
 972 However, in a reality the positions and tilts of the modules are different from ones suggested by  
 973 the ideal geometry (Fig. 24, middle right). Hits, indeed, are recorded at the places where mod-  
 974 ules are actually mounted, not at the design ideal places (Fig. 24, bottom left). If we assumed a  
 975 tracker to be ideal and a track to be smooth, we would see that our hits are off-track (Fig. 24,  
 976 bottom right). So, we recalculate positions of the modules so that all the hits are laying on the  
 977 same smooth track (Fig. 25, top left). But these recalculated positions still do not coincide with  
 978 the actual positions (Fig. 25, top right). Then we record more and more tracks (Fig. 25, middle  
 979 left and right). We take into account them all and determine the alignment parameters with  
 980 necessary precision (Fig. 25, bottom left and right).

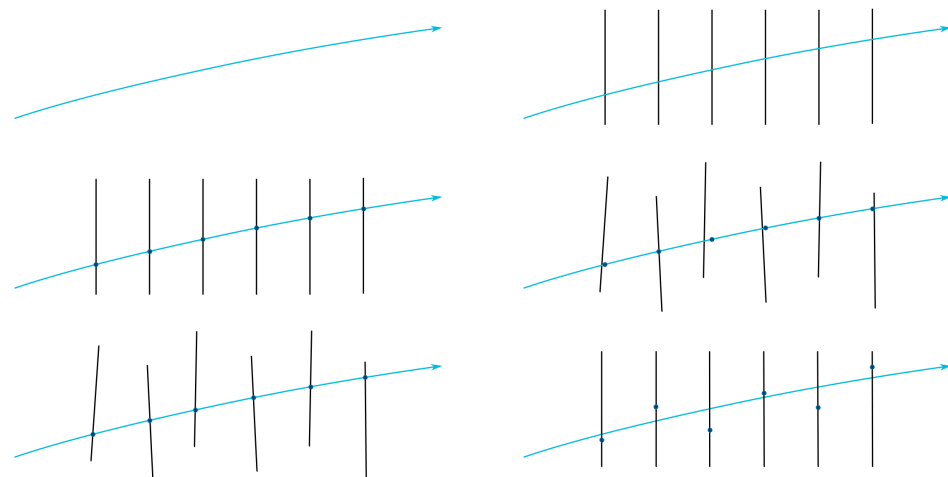


Figure 24: The alignment of a toy tracker, part 1.

985 When we record a track with a not-aligned tracker, we see that the track is not smooth. But

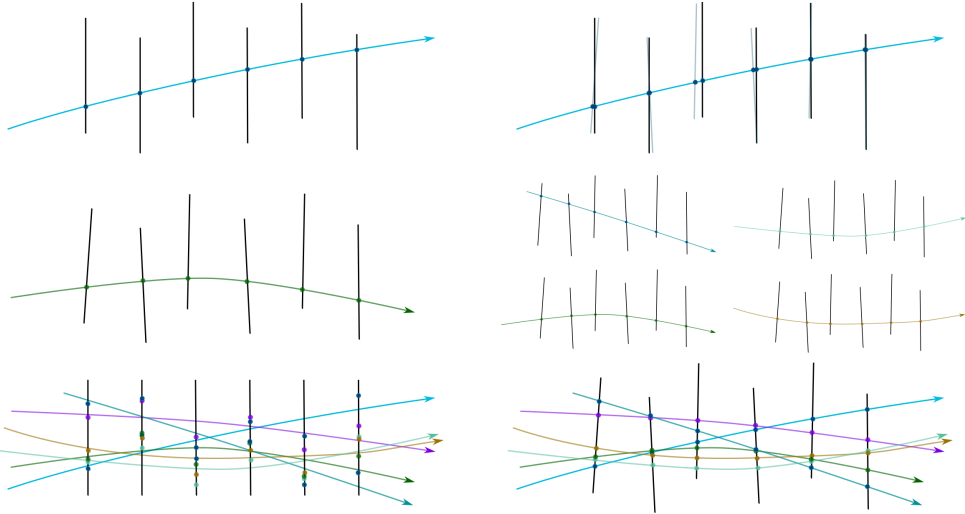


Figure 25: The alignment of a toy tracker, part 2.

that is because our knowledge of module positions is not exact. Thus, we can correct the positions assuming the track is smooth. But when we process the next track, we may find out that the positions have to be corrected again. Thus, we record many tracks and minimize residuals between measured and predicted hits.

The CMS tracker contains 1440 silicon pixel modules in PXB and PXF and 15148 silicon strip modules in TIB, TOB, TID, TEC.

The tracker alignment problem is the least squared problem. The expression to minimize is the following:

$$\chi^2(\mathbf{p}, \mathbf{q}) = \sum_j^{\text{tracks}} \sum_i^{\text{tracks}} \left( \frac{m_{ij} - f_{ij}(\mathbf{p}, \mathbf{q}_j)}{\sigma_{ij}} \right)^2 \quad (36)$$

where  $\mathbf{p}$  are parameters describing the tracker geometry,  $\mathbf{q}_j$  are parameters of the  $j^{th}$  track,  $m_{ij} - f_{ij}$  are residuals, distances between the measured hit and a position predicted by the track fit,  $\sigma_{ij}$  is the Gaussian error of the measurement.

We can align the large substructures and individual modules with respect to their substructures. The parameters to align large substructures include their positions and orientations of the subdetectors (rotations). Thus, each subsystem is described by six parameters: three coordinates X, Y, Z and three angles  $\alpha$ ,  $\beta$ ,  $\gamma$ . At the module level, we align positions and rotations with respect to the position s and angles of the corresponding large structure (Fig. 26). In addition, at the module level we align for surface deformations which are described by three parameters per sensor (Fig. 27).

A track can be described with five parameters.

We have two alignment algorithms: Millepede and HIP. Millepede performs a simultaneous fit of all alignment parameters and all track parameters while HIP perform iterative fits of alignment parameters  $\mathbf{p}$  and track parameters  $\mathbf{q}_j$ .

It is important to use different sorts of tracks for the alignment. Cosmic tracks pass through the detector vertically and do not allow us to connect different subdetectors to one another.

1016 Collision tracks originate from the collision point and go in all directions. However, those tracks  
 1017 which cross TEC are all almost collinear and, therefore, it is difficult to measure  $z$ -coordinate of  
 1018 TEC modules with collision tracks only.

1019

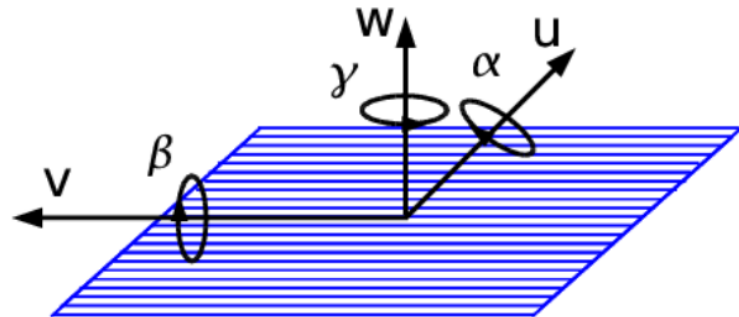


Figure 26: Alignment parameters.

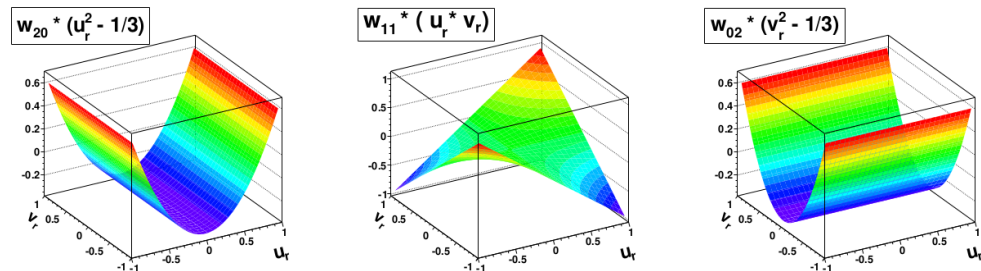


Figure 27: Surface deformations.

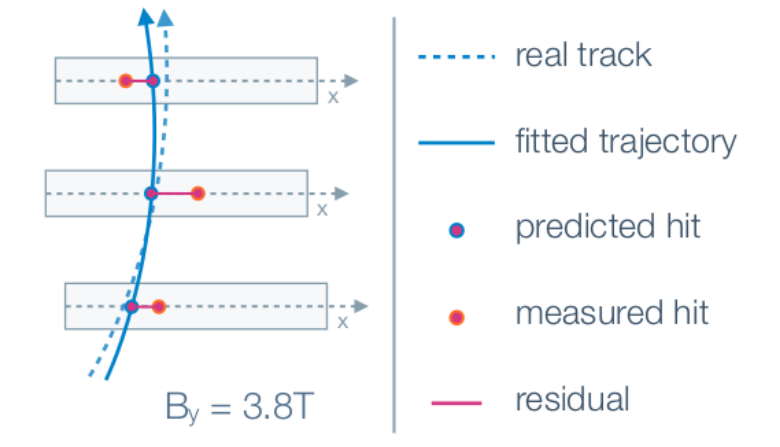


Figure 28: Track residuals.

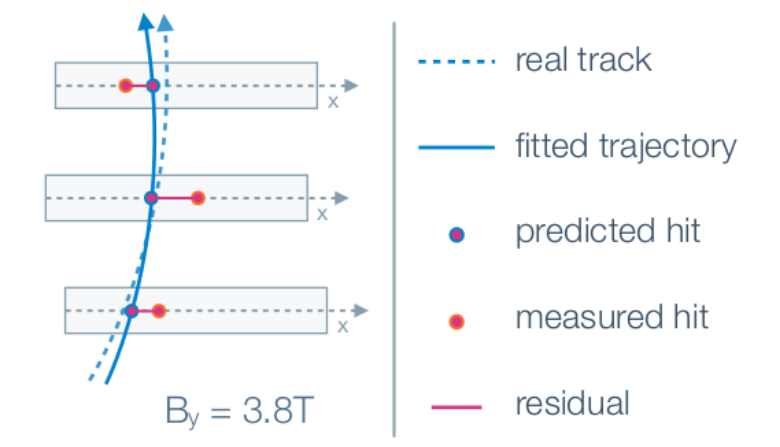


Figure 29: Track residuals.

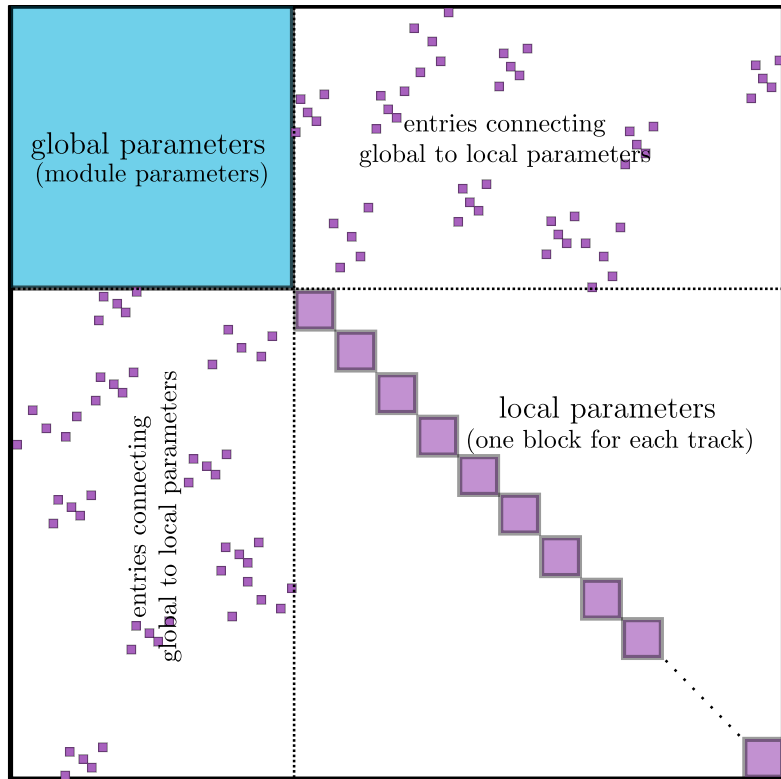


Figure 30: Track residuals.

1020 **4.2 Selected Results**

1021 CRUZET, CRAFT and first collisions of 2015

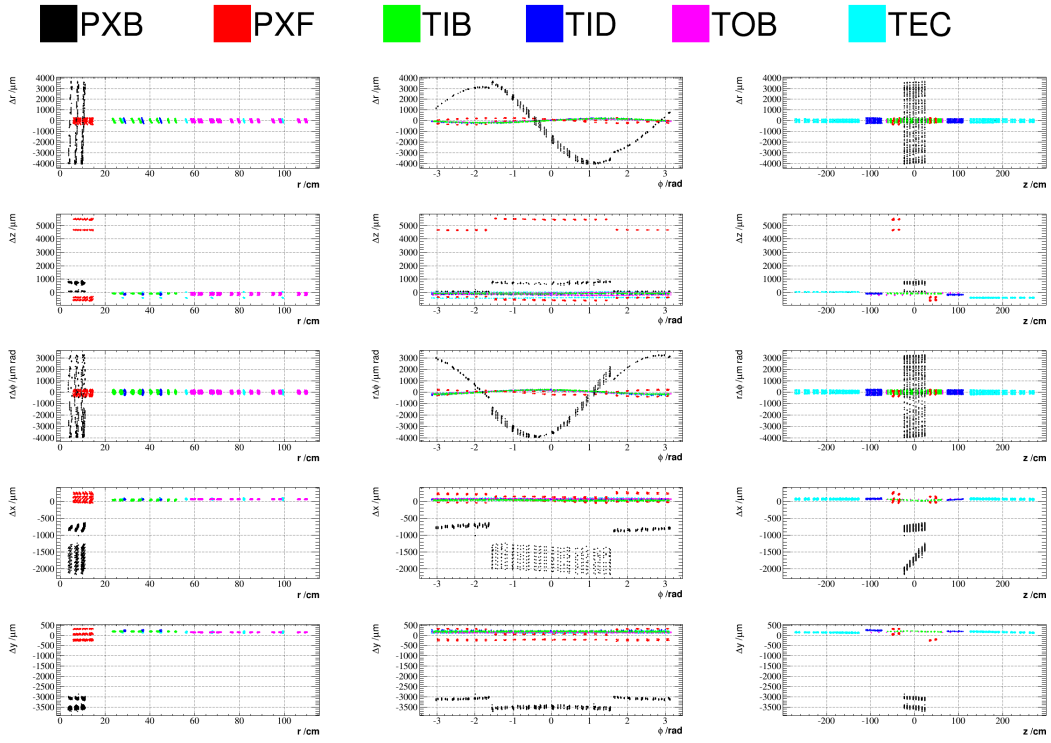


Figure 31: Geometry comparison plot of CRUZET 2015 object vs Run I.

**5  $W\gamma$  Cross Section Measurement**

1022 Place analysis outline here  
1023

---

## References

- [1] Griffiths textbook
- [2] website: <http://www.isgtw.org/spotlight/go-particle-quest-first-cern-hackfest>
- [3] CMS Paper about Higgs boson discovery
- [4] ATLAS Paper about Higgs boson discovery
- [5] PDG
- [6] website: <https://science.nasa.gov/astrophysics/focus-areas/what-is-dark-energy>
- [7] Pich lectures: The Standard Model of Electroweak interactions
- [8] Halzen, Martin "Quarks and leptons"
- [9] <http://iopscience.iop.org/article/10.1088/0034-4885/70/1/R02>
- [10] Peskin, Schroeder
- [11] Lindsey's thesis (CMS Zg- $\zeta$ llg, 7 TeV)
- [12] website: [https://www-d0.fnal.gov/results/publications\\_talks/thesis/snyder/html/node17.html](https://www-d0.fnal.gov/results/publications_talks/thesis/snyder/html/node17.html)
- [13] website: [https://en.wikipedia.org/wiki/Cross\\_section\\_%28physics%29](https://en.wikipedia.org/wiki/Cross_section_%28physics%29)
- [14] LO (1969) theory paper
- [15] NNLO theory paper
- [16] NLO theory paper
- [17] aTGC paper
- [18] Senka's thesis (CMS Wg- $\zeta$ munug, 7 TeV)
- [19] D0 Combination of  $W\gamma$ , WW, WZ and VW using 8.6 fb-1 of 2 TeV  $p\bar{p}$  collisions Phys.Lett. B718 (2012) 451-459
- [20] LEP Combination of WW and single W using 0.7 fb-1 per experiment of  $e^+e^-$  collisions at WW pair production energies arXiv:1302.3415
- [21] 7TeV Wg ATLAS paper
- [22] ATLAS WW using 20.3 fb-1 of 8 TeV pp collisions Submitted to JHEP
- [23] ATLAS VW ( $V=W,Z \rightarrow jj$ ) using 4.6 fb-1 of 7 TeV pp collisions JHEP 01 (2015) 049
- [24] website: [https://twiki.cern.ch/twiki/bin/view/CMSPublic/PhysicsResultsSMPaTGC#Figure\\_1\\_Limits\\_on\\_WW](https://twiki.cern.ch/twiki/bin/view/CMSPublic/PhysicsResultsSMPaTGC#Figure_1_Limits_on_WW)
- [25] 7TeV Wg CMS paper
- [26] CMS WW using 4.9 fb-1 of 7 TeV pp collisions Eur. Phys. J. C 73 (2013) 2610
- [27] CMS WW using 19.4 fb-1 of 8 TeV pp collisions Submitted to EPJC
- [28] CMS VW ( $V=W,Z \rightarrow jj$ ) using 5.0 fb-1 of 7 TeV pp collisions Eur.Phys.J. C73 (2013) 2283
- [29] CMS 8 TeV WW lnlnmu
- [30] CMS 7 TeV Zg nunug
- [31] CERN brochure, <http://cds.cern.ch/record/1165534/files/CERN-Brochure-2009-003-Eng.pdf>

- 1059 [32] LHC TDR
- 1060 [33] website: <http://home.cern/topics/large-hadron-collider>
- 1061 [34] website: <http://cds.cern.ch/record/1621583/files/>
- 1062 [35] [http://home.cern/sites/home.web.cern.ch/files/image/update-for\\_cern\\_people/2016/06/intlumirunall\\_image.png](http://home.cern/sites/home.web.cern.ch/files/image/update-for_cern_people/2016/06/intlumirunall_image.png)
- 1063 [36] website: <http://cds.cern.ch/journal/CERNBulletin/2014/24/News%20Articles/1706606>
- 1064 [37] website: <https://twiki.cern.ch/twiki/bin/view/CMSPublic/LumiPublicResults>
- 1065